Editors' Suggestion

Strong-coupling superconductivity near Gross-Neveu quantum criticality in Dirac systems

Veronika C. Stangier,[1] Daniel E. Sheehy,[2] and Jörg Schmalian[1,3]
[1]*Institute for Theory of Condensed Matter, Karlsruhe Institute of Technology, Karlsruhe 76131, Germany*
[2]*Department of Physics and Astronomy, Louisiana State University, Baton Rouge, Louisiana 70803, USA*
[3]*Institute for Quantum Materials and Technologies, Karlsruhe Institute of Technology, Karlsruhe 76131, Germany*

(Received 13 October 2025; revised 27 November 2025; accepted 15 December 2025; published 10 February 2026)

We study two-dimensional massless Dirac fermions at neutrality, coupled to bosonic modes through a Yukawa interaction. We then examine the intriguing possibility that such a system, devoid of carriers at zero temperature, might nevertheless exhibit superconductivity. Remarkably, we find that superconductivity emerges in the vicinity of Gross-Neveu quantum criticality, provided the fermions cease to behave as well-defined quasiparticles, that is, once their anomalous dimension in the normal state becomes sufficiently large. In other words, well-defined fermions do not superconduct, whereas ill-defined ones do. We analyze four symmetry-distinct bosonic modes, each capable of driving normal-state criticality and, in three of the four cases, giving rise to a distinct superconducting phase. While phase fluctuations are strong in this regime, we argue that they do not destroy the superconducting state. We further characterize the resulting pairing states for a concrete Dirac model of spin-orbit coupled systems with orbitals of different parity. Our results are obtained using the Sachdev-Ye-Kitaev (SYK)-inspired framework for Dirac systems introduced by Kim *et al.* [Dirac fast scramblers, Phys. Rev. B **103**, L081113 (2021)], which provides a controlled approach to the strongly coupled regime of Dirac fluids near Gross-Neveu criticality.

DOI: 10.1103/x7lc-ztqn

I. INTRODUCTION

The exploration of two-dimensional gapless Dirac materials [1–3], i.e., systems in which low-energy excitations mimic relativistic, Dirac fermions, is of importance in several prominent materials such as single layer graphene [4,5], twisted bilayer graphene [6–9], twisted double-layer WSe_2 [10–14], surface states of three-dimensional topological insulators [15,16], near-ferroelectric semimetals [17,18], or in the case of merging Dirac points [19–22]. Near the neutrality point of a massless Dirac fermion, the density of states at the Fermi level is small, which makes Dirac systems comparatively robust against weak interactions. However, at strong coupling Gross-Neveu (GN) quantum criticality [23,24] has received significant attention [25–39]. At the GN critical point, fermions spontaneously acquire a mass as a consequence of spontaneous symmetry breaking. In single-layer graphene, sufficiently strong Coulomb interaction was expected to break the sublattice symmetry that protects the Dirac point [25–30]. The magnitude of the fine-structure constant in this system does not, however, appear to be sufficiently large to reach the GN critical point. The situation is more promising in twisted two-dimensional materials, such as twisted double-layer WSe_2 [13], which is considered an effective strongly-correlated version of single-layer graphene [10,11], or in twisted bilayer graphene (TBG) [37,38]. In both systems one expects a spontaneous mass generation at neutrality as function of the twist angle. The nature of the insulating state in WSe_2 is unclear with some evidence favoring a magnetic state [13]. In TBG there are arguments in favor of an intervalley-coherent insulator [40–42] that was observed in experiment, albeit at a different filling [43].

The mass generation at a GN-critical point is accompanied by strong quantum fluctuations that give rise to anomalous dimensions η_ψ and η_ϕ of the fermions and mass-generating collective bosons, respectively. They are defined through the infrared momentum dependence of the fermionic [$G(k)$] and bosonic [$D(k)$] propagators:

$$G(k_\mu) \propto -i\frac{k_\mu \gamma^\mu}{|k|^{2-\eta_\psi}}, \tag{1}$$

$$D(k_\mu) \propto \frac{1}{|k|^{2-\eta_\phi}}. \tag{2}$$

$k_\mu = (\omega/v_F, k_x, k_y)$ is the (Euclidean) three-vector of magnitude $|k|$ and γ^μ are the 4×4 Dirac matrices. When η_ψ is finite (and not parametrically small) the critical fermions, described by Eq. (1), are no longer well-defined quasiparticles. The potential implications of this breakdown of the quasiparticle picture and the possibility of superconductivity masking the GN-critical point are the main foci of this paper.

Analytic approaches to determine η_ψ and η_ϕ at GN criticality are usually based on expansions in small $\epsilon = 3 - d$ or $1/N$, where N is the number of fermion flavors [24]. Specifically, one obtains to leading order in ϵ or $1/N$ the results $\eta_\psi \sim \mathcal{O}(\epsilon) \sim \mathcal{O}(1/N)$ and $\eta_\phi \sim \mathcal{O}(\epsilon) \sim 1 - \mathcal{O}(1/N)$ [24,33]. Hence, in the limit of many fermion flavors, the critical boson behaves in a highly non-Gaussian manner while fermionic Dirac particles at criticality are almost well-defined fermionic excitations. Both are well-defined near three space

Published by the American Physical Society under the terms of the Creative Commons Attribution 4.0 International license. Further distribution of this work must maintain attribution to the author(s) and the published article's title, journal citation, and DOI.

dimensions. Monte Carlo simulations for $d = 2$ [34,39,44], conformal bootstrap approaches [45], high-loop expansion in ϵ [33], as well as functional renormalization group approaches [46,47], all yield values for the anomalous fermion dimension that range, depending on the problem under consideration up to $\eta_\psi \sim 0.17$. Hence, in two dimensions fermions at the GN-quantum critical point are in fact ill-defined quasiparticles.

Recently, an analytic strong-coupling approach to Dirac systems was proposed in Ref. [48] as a generalization of a zero-dimensional Yukawa-Sachdev-Ye-Kitaev model [49–56]. The system displays quantum chaos [48] akin to what was observed in black hole problems [57]. For closely related strong-coupling approaches to compressible Fermi systems, see Refs. [56,58–62]. The model of Ref. [48] contains M real scalar boson fields and N four-component Dirac fermions, interacting via a Yukawa interaction. Crucially, the couplings of this interaction are Gaussian random numbers that are the same everywhere in space, i.e., translation invariance is not broken, even for a specific realization of the coupling constants. Analyzing the averaged model then allows for large M and N to obtain analytic control of a strong coupling fixed point with a fermionic anomalous dimension that is not parametrically small. The detailed properties of the fixed point depend on the ratio M/N, where the behavior near $M \ll N$ behaves similar to the above large-N limit with $\eta_\psi \sim \mathcal{O}(M/N)$ and $\eta_\phi \sim 1 - \mathcal{O}(M/N)$, while $M \gg N$ yields $\eta_\psi \sim \frac{1}{2} - \mathcal{O}(N/M)$ and $\eta_\phi \sim \mathcal{O}(N/M)$. Hence, within this approach, fermions indeed possess a sizable anomalous dimension $0 < \eta_\psi < \frac{1}{2}$ and are no-longer well-defined quasiparticles. Reference [48] also demonstrated quantitative agreement of the anomalous exponents obtained from the generalized Sachdev-Ye-Kitaev (SYK) approach with results obtained using conformal bootstrapping approaches [45].

In this paper we generalize the approach of Ref. [48] to include superconductivity and analyze whether strong quantum fluctuations and nonquasiparticle behavior of the fermions give rise to superconductivity as a secondary instability. Hence, we examine the intriguing possibility that such a system, devoid of carriers at zero temperature, might nevertheless exhibit superconductivity. In our approach, superconductivity is driven by fluctuations of the bosons whose eventual condensation generates the fermion mass. Hence, the pairing "glue" in our system arises from the exchange of the same collective, mass-generating boson that give rise to the anomalous dimensions in the first place. The essential differences to conventional, e.g., phonon-driven pairing in compressible systems are are that the boson in our case is critical, and that the Dirac system at charge neutrality has a vanishing density of states at the Fermi level. The latter makes strong-coupling effects a necessary condition for superconductivity. Interestingly we find that superconductivity occurs provided that the anomalous fermion dimension exceeds a threshold value which in our theory turns out to be

$$\eta_\psi^c \approx 0.14628. \tag{3}$$

Hence, we obtain the curious result that well-defined quasiparticles do not superconduct while ill-defined ones do. Whether the precise value of η_ψ^c is indeed the correct one to compare with numerical work on GN models is unclear, given that

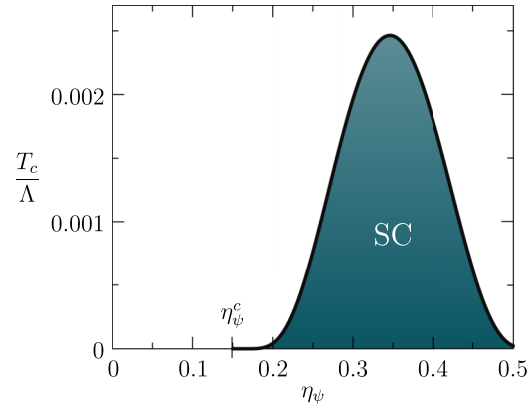

FIG. 1. Superconducting transition temperature T_c as function of the anomalous dimension η_ψ of the fermions at the Gross-Neveu mass-generating transition of two-dimensional Dirac systems within the generalized SYK approach of this paper. For system with η_ψ larger than a threshold value η_ψ^c, fluctuations of the mass-generating boson give rise to a superconducting instability, where the largest T_c occurs at intermediate values of η_ψ. Λ is the upper cut off of the Dirac theory.

we are really only solving an approximate strong-coupling theory. What is more important is the very existence of such a threshold value for superconductivity that is comparable to values in two-dimensional systems. The resulting behavior for $\eta_\psi > \eta_\psi^c$ is illustrated in Fig. 1, where we show the superconducting transition temperature [as determined in Eq. (66) below] as function of η_ψ. We expect superconductivity only near the critical GN transition $g = g_c$, forming a dome whose maximum transition temperature occurs at or very close to the GN critical point. Below g_c superconductivity must disappear at some threshold value [63,64], while T_c should vanish in the gapped phase above g_c. Hence, we expect that GN criticality should be accompanied by pairing or, at the very least, by enhanced pairing fluctuations. Moreover, our analysis shows how to identify the critical bosonic modes most likely to give rise to an unconventional pairing state. In this context is it an interesting question to explore whether the superconductivity identified here is related to the seeds of pairing in the ordered state of some Dirac systems where skyrmion configurations of the order parameter were shown to be charge-2e degrees of freedom [42,65–69].

We explore generic four-component Dirac spinors, systematically analyze the full set of interactions that can drive the system into a quantum critical regime, identify the leading pairing instabilities that emerge, and discuss the role of phase fluctuations. To facilitate the identification of possible superconducting states, we present generic algebraic conditions on the spinor structure of the pairing state, formulated for an arbitrary Dirac theory with a general number of spinor components coupled to a fully general set of critical bosons. In this context we demonstrate that no pairing arises in the simplest $2+1$-dimensional Dirac theory with a single two-component spinor. Broadly speaking, the more intricate the Dirac structure, the more readily pairs can form in a manner consistent with Fermi statistics. This point will be made particularly clear in a separate note [70], which investigates the

pairing states of Dirac models for twisted double-layer WSe_2 and twisted bilayer graphene near Gross-Neveu criticality.

II. MODEL AND LARGE-N, M SADDLE POINT

A. The model, symmetries, and Dirac spinor structure

Following Ref. [48], we consider the Hamiltonian of N massless Dirac electrons, each described by a four component Dirac spinor $\psi_l(\boldsymbol{x})$ and additional N flavors, i.e., $l = 1 \cdots N$, that interact with M massive scalar bosonic modes $\phi_s(\boldsymbol{x})$ with $s = 1 \cdots M$. The Hamiltonian of the problem is then given as

$$\begin{aligned} H = & v_{\mathrm{F}} \sum_{l=1}^{N} \int d^2x \psi_l^\dagger(\boldsymbol{x})(-i\nabla)\cdot\boldsymbol{\alpha}\psi_l(\boldsymbol{x}) \\ & + \frac{1}{2}\sum_{s=1}^{M}\int d^2x\left(\pi_s^2(\boldsymbol{x}) + \omega_0^2\phi_s^2(\boldsymbol{x}) + v_{\mathrm{B}}^2(\nabla\phi_s(\boldsymbol{x}))^2\right) \\ & + \frac{1}{N}\sum_{lms}\int d^2x(g_{lm,s}\psi_l^\dagger(\boldsymbol{x})\Upsilon\psi_m(\boldsymbol{x})\phi_s(\boldsymbol{x}) + \mathrm{H.c.}), \end{aligned} \tag{4}$$

where $\psi_l(\boldsymbol{x})$ is a four-component Dirac spinor with the additional flavor index $l = 1 \cdots N$. π_s is the conjugated momentum to the boson field ϕ_s, i.e., $[\phi_s(\boldsymbol{x}), \pi_{s'}(\boldsymbol{x}')] = i\delta_{s,s'}\delta(\boldsymbol{x} - \boldsymbol{x}')$. v_{F} and v_{B} are the fermionic and bosonic velocities. The 4×4 Dirac matrices hold the usual properties $\{\alpha_i, \alpha_j\} = 2\delta_{ij}$, $\{\alpha_i, \beta\} = 0$, and $\beta^2 = 1$. Curly brackets stand for the anticommutator. In our analysis we will also use the Euclidean covariant formulation with $\gamma^0 = \beta$ and $\gamma^i = -i\beta\alpha_i$. They obey $\{\gamma^\mu, \gamma^\nu\} = 2\delta^{\mu\nu}$. In what follows we set $v_{\mathrm{F}} = 1$, while the magnitude of the boson velocity will not enter the universal low-energy behavior. Within the approach of this paper, the additional inclusion of a nonlinear, ϕ^4, term in the Hamiltonian will not change the universal behavior and is therefore ignored at the outset.

The fermion-boson coupling is determined by the 4×4 matrix Υ. We consider four different Hermitian coupling matrices Υ_i, $i = 1 \cdots 4$, where boson condensation induces a gap with the usual spectrum

$$E = \pm\sqrt{p^2 + m_{\mathrm{F}}^2}, \tag{5}$$

and fermion mass $m_{\mathrm{F}} \propto \langle\phi\rangle$. This is obviously the case for $\Upsilon_1 = \gamma^0$. In total there are four possible interactions that anticommute with α^1 and α^2 and hence induce, upon condensation of ϕ, an isotropic gap at the Dirac point as in Eq. (5):

$$\{\Upsilon_1, \Upsilon_2, \Upsilon_3, \Upsilon_4\} = \{\gamma^0, i\gamma^0\gamma^3, i\gamma^1\gamma^2, i\gamma^0\gamma^5\}, \tag{6}$$

with $\gamma^5 = \gamma^0\gamma^1\gamma^2\gamma^3$. The transformation of these coupling matrices under parity and time reversal are listed in Table I below. Notice, we consider a $2+1$ dimensional system. $\Upsilon_1 = \gamma^0$ and $\Upsilon_4 = i\gamma^0\gamma^5$ are allowed coupling matrices even if one included the third spatial dimension. They correspond to the usual and chiral mass of $3+1$-dimensional Dirac systems [71]. $\Upsilon_2 = i\gamma^0\gamma^3$ and $\Upsilon_3 = i\gamma^1\gamma^2$ are additional coupling terms that only exist in two dimensions. Another distinction of these two pairs of couplings is that $\Upsilon_{1,4}$ anticommute with γ^5 (flip chirality) while $\Upsilon_{2,3}$ commute with γ^5 (preserve chirality), i.e., $\Upsilon_i\gamma^5 = b_i\gamma^5\Upsilon_i$, with $b_{1,4} = -1$ and $b_{2,3} = 1$.

TABLE I. Four different coupling interactions Υ_i along with the transformation of the critical boson ϕ under parity (p_ϕ) and time reversal (τ_ϕ). In addition we show the matrix structure of the pairing interaction l_J for $J \in \{S, V, A, P\}$. Q refers to the 3×3 block $Q_{\mu\nu} = 2q^\mu q^\nu/q^2 - \delta^{\mu\nu}$. In green we show the interactions that give rise to pairing. For $\Upsilon_i = i\gamma^1\gamma^2$ the anisotropic interaction Q, marked in red and due to the pairing in the l_V channel, is the dominant pairing interaction. However, its pairing strength is always smaller than the threshold coupling value λ_p^c, i.e., no superconducting state emerges for this interaction and one might at best observe enhanced pairing fluctuations. The last row shows the spinor structure of the pairing self-energy Φ.

Υ_i	γ^0	$i\gamma^0\gamma^3$	$i\gamma^1\gamma^2$	$i\gamma^0\gamma^5$
p_i	1	-1	1	-1
τ_i	1	-1	-1	-1
b_i	-1	1	1	-1
l_S	1	1	1	1
l_V	$\begin{pmatrix} Q & \\ & -1 \end{pmatrix}$	$\begin{pmatrix} -Q & \\ & -1 \end{pmatrix}$	$\begin{pmatrix} Q & \\ & 1 \end{pmatrix}$	$\begin{pmatrix} -Q & \\ & 1 \end{pmatrix}$
l_A	$\begin{pmatrix} -Q & \\ & 1 \end{pmatrix}$	$\begin{pmatrix} -Q & \\ & -1 \end{pmatrix}$	$\begin{pmatrix} Q & \\ & 1 \end{pmatrix}$	$\begin{pmatrix} Q & \\ & -1 \end{pmatrix}$
l_P	-1	1	1	-1
Φ	1	γ^3	$-$	γ^5

Finally we discuss the random coupling constants g_{lms}. Following Refs. [53,55], we consider real coupling constants with

$$\overline{g_{lms}g_{l'm's'}} = g^2\delta_{ss'}(\delta_{ll'}\delta_{mm'} + \delta_{lm'}\delta_{ml'}). \tag{7}$$

The fact that the coupling constants are $\boldsymbol{x}$ independent implies that translation invariance is not broken, even for specific realizations of the g_{lms}. In other words we consider the average of an ensemble of interacting systems with slightly different values of the coupling constant. This rather peculiar large-N, M limit has the advantage that it offers controlled insights into the strong-coupling behavior of Yukawa-coupled theories.

Before we analyze the Dirac problem we collect some information of its behavior under symmetry operations. This will prove useful for the analysis of the pairing states. We consider a problem without broken parity and time-reversal symmetry on the level of the Hamiltonian. Let $\mathcal{R}$ be a spatial symmetry operation of the problem, it holds in momentum space:

$$\begin{aligned} \psi(\boldsymbol{k}) &\xrightarrow{\mathcal{R}} u_R\psi\left(R_v^{-1}\boldsymbol{k}\right), \\ \psi^\dagger(\boldsymbol{k}) &\xrightarrow{\mathcal{R}} \psi^\dagger\left(R_v^{-1}\boldsymbol{k}\right)u_R^\dagger, \\ \phi(\boldsymbol{k}) &\xrightarrow{\mathcal{R}} u_{\phi,R}\phi\left(R_v^{-1}\boldsymbol{k}\right), \end{aligned} \tag{8}$$

with R_v, u_R, and $u_{\phi,R}$ the vector, spinor, and bosonic field representation of $\mathcal{R}$, respectively. Here we suppressed the additional flavor indices l and s for simplicity. For fermionic bilinear combinations

$$I_O = \int d^dk\psi^\dagger(\boldsymbol{k})O(\boldsymbol{k})\psi(\boldsymbol{k}), \tag{9}$$

it holds that the single particle operator O, which is a 4×4 matrix in spinor space, transforms like $O(\boldsymbol{k}) \xrightarrow{\mathcal{R}} u_R^\dagger O(R_v\boldsymbol{k})u_R$.

Parity transformation is given as

$$\begin{aligned}\psi(\boldsymbol{k}) &\xrightarrow{\mathcal{P}} u_P\psi(-\boldsymbol{k}),\\ \psi^\dagger(\boldsymbol{k}) &\xrightarrow{\mathcal{P}} \psi^\dagger(-\boldsymbol{k})u_P^\dagger,\\ \phi(\boldsymbol{k}) &\xrightarrow{\mathcal{P}} p_i\phi(-\boldsymbol{k}),\end{aligned} \tag{10}$$

with $u_P = \beta = \gamma^0$. $p_i = \pm 1$ is the boson parity that depends on the choice of the coupling matrix Υ_i. For $\Upsilon_1 = \beta$ the boson is of even parity. More generally follows that $u_P\Upsilon_i u_P^\dagger = p_i\Upsilon_i$.

Time reversal, $\mathcal{T} = \mathcal{K}U_T^\dagger$ is the combination of complex conjugation $\mathcal{K}$ and a unitary operator U_T. In our model it corresponds for the fermion and boson operators to

$$\begin{aligned}\psi(\boldsymbol{k},t) &\xrightarrow{\mathcal{T}} u_T\psi(-\boldsymbol{k},-t),\\ \psi^\dagger(\boldsymbol{k},t) &\xrightarrow{\mathcal{T}} \psi^\dagger(-\boldsymbol{k},-t)u_T^\dagger,\\ \phi(\boldsymbol{k},t) &\xrightarrow{\mathcal{T}} \tau_i\phi(-\boldsymbol{k},-t),\end{aligned} \tag{11}$$

with $\tau_i = \pm 1$ the parity of the boson under time reversal, which depends on the choice of Υ_i. u_T is the spinor representation of U_T and the operators are given in the Heisenberg picture. To ensure that the Hamiltonian is time reversal symmetric it must hold

$$\begin{aligned}u_T^\dagger\boldsymbol{\alpha}^* u_T &= -\boldsymbol{\alpha},\\ u_T^\dagger\beta^* u_T &= \beta,\\ u_T^\dagger\Upsilon_i^* u_T &= \tau_i\Upsilon_i.\end{aligned} \tag{12}$$

The specific representation of u_T depends on the choice of the Dirac matrices. Since time reversal for the fermions squares to $\mathcal{T}^2 = -1$ it holds $u_T^* u_T = -1$ and, using $u_T^\dagger u_T = 1$, it follows that $u_T^T = (u_T^{-1})^* = -u_T$. Time reversal is not a spatial symmetry and must, hence, commute with all operations of the symmetry group, $[\mathcal{R},\mathcal{T}] = 0$. This implies for the spinor representation$[u_T^\dagger\mathcal{K}, u_R] = 0$ for all symmetry operations $\mathcal{R}$, and leads to

$$u_T^\dagger u_R^* = u_R u_T^\dagger, \tag{13}$$

a relation that will prove handy as we describe pairing instabilities.

In the context of superconductivity, one encounters anomalous bilinear forms of the kind

$$I_\Delta = \int d^dk\,\psi^\dagger(\boldsymbol{k})\Delta(\boldsymbol{k})(\psi^\dagger(-\boldsymbol{k}))^T \tag{14}$$

or its Hermitian conjugate. Because of the two creation operators, it now follows that under symmetry transformations $\Delta(\boldsymbol{k}) \xrightarrow{\mathcal{R}} u_R^\dagger\Delta(R_v\boldsymbol{k})u_R^*$. This is distinct from the behavior of a usual fermion bilinear and not very convenient. It can be avoided if we use, instead of Δ, the quantity

$$\Phi(\boldsymbol{k}) = \Delta(\boldsymbol{k})u_T^\dagger. \tag{15}$$

Using Eq. (13), which relates spatial symmetry operations and time reversal, one easily finds that Φ transforms like a usual bilinear form

$$\Phi(\boldsymbol{k}) \xrightarrow{\mathcal{R}} u_R^\dagger\Phi(R_v\boldsymbol{k})u_R. \tag{16}$$

It is this property that makes the Nambu spinor

$$\Psi(\boldsymbol{k}) = \begin{pmatrix}\psi(\boldsymbol{k})\\ u_T^\dagger(\psi^\dagger(-\boldsymbol{k}))^T\end{pmatrix} \tag{17}$$

the natural, symmetry-adapted description of a superconductor.

For the subsequent analysis of pairing states, it will prove convenient to expand generic Hermitian 4×4 matrices in terms of 16 base matrices; see e.g. Refs. [71,72]:

$$\begin{aligned}&\Gamma_S = 1, \quad \Gamma_V^\mu = \gamma^\mu, \quad \Gamma_T^{\mu\nu} = \sigma^{\mu\nu}\ \ \mu<\nu,\\ &\Gamma_A^\mu = i\gamma^\mu\gamma_5, \quad \Gamma_P = \gamma_5,\end{aligned} \tag{18}$$

with $\sigma^{\mu\nu} = \frac{i}{2}[\gamma^\mu,\gamma^\nu]$. S, V, T, A, and P stand for scalar, vector, (antisymmetric) tensor, axial vector, and pseudoscalar, respectively. It holds $\frac{1}{4}\mathrm{tr}(\Gamma_I^r\Gamma_J^{r'}) = \delta_{I,J}\delta_{r,r'}$ as well as $(\Gamma_J^r)^2 = 1$. The coupling matrices of Eq. (6) are $\Upsilon_i \in \{\Gamma_V^0, \Gamma_T^{03}, \Gamma_T^{12}, \Gamma_A^0\}$. Under time reversal, Γ_S, Γ_V^μ, and Γ_P are even, while $\Gamma_T^{\mu\nu}$ and Γ_A^μ are odd. In addition Γ_S, Γ_V^0, Γ_T^{ij} and Γ_A^i are even under parity while Γ_V^i, Γ_T^{0i}, Γ_A^0, and Γ_P are odd under parity. Here, the superscript i stands for the spatial components.

B. Large-N, M saddle point equations

The analysis of the large-N, M equations is a direct extension of the approach of Refs. [53,54,56]. We perform the replica trick to average over the random variables g_{lms}, drawn from a Gaussian ensemble governed by Eq. (7), and take the replica-symmetric limit. We then introduce the bilocal fields (G and F have a 4×4 matrix structure)

$$\begin{aligned}G(x,x') &= \frac{1}{N}\sum_l \psi_l(x)\odot\psi_l^\dagger(x'),\\ F(x,x') &= \frac{1}{N}\sum_l \psi_l(x)\odot(\psi_l(x')u_T),\\ D(x,x') &= \frac{1}{M}\sum_s \phi_s(x)\phi_s(x'),\end{aligned} \tag{19}$$

that describe normal and pairing correlations of the fermions as well as bosonic correlations. $x = (\tau,\boldsymbol{x})$ combines imaginary time and spatial coordinates. In our definition of the anomalous function F we added u_T, following the discussion that led to Eq. (15).

Integrating out the primary fields gives rise to the saddle point equations in the limit of large N and M at fixed N/M. As we have to include pairing terms in the analysis, see Ref. [53], we use the Nambu spinor of Eq. (17). At the saddle point it holds that

$$\Sigma(x) = g^2\frac{M}{N}\Upsilon_i G(x)\Upsilon_i D(x), \tag{20}$$

$$\Phi(x) = -\tau_i g^2\frac{M}{N}\Upsilon_i F(x)\Upsilon_i D(x), \tag{21}$$

$$\begin{aligned}\Pi(x) = &-g^2\mathrm{tr}(\Upsilon_i G(x)\Upsilon_i G(-x))\\ &+\tau_i g^2\mathrm{tr}(\Upsilon_i\bar{F}(x)\Upsilon_i F(-x)).\end{aligned} \tag{22}$$

τ_i is the transformation of the boson ϕ, and hence of the coupling matrix Υ_i, under time reversal; see Eq. (12). Σ, Φ, and Π formally enter the theory as Lagrange-parameter fields

that enforce Eq. (19). At the saddle point they play the role of the fermionic and bosonic self-energies and are determined by the Dyson equations which we write in the frequency and momentum domain with $k = (\omega, \boldsymbol{k})$ as

$$\hat{G}^{-1}(k) = \hat{G}_0^{-1}(k) - \hat{\Sigma}(k), \tag{23}$$

where

$$\hat{G}(k) = \begin{pmatrix} G(k) & F(k) \\ \bar{F}(k) & -u_T^\dagger G^T(-k) u_T \end{pmatrix}, \tag{24}$$

and similar structure for $\hat{\Sigma}$ in terms of Σ and Φ. The inverse of the bare fermionic propagator in Nambu space is

$$\hat{G}_0^{-1}(k) = \begin{pmatrix} ik_\mu \gamma^\mu \gamma^0 & 0 \\ 0 & ik_\mu \gamma^0 \gamma^\mu \end{pmatrix}. \tag{25}$$

The bosonic Dyson equation is given as

$$D(q) = \frac{1}{\omega_0^2 + q^2 - \Pi(q)}. \tag{26}$$

C. Normal state analysis

We first analyze the solution of the saddle-point equations in the normal state where $\Phi = F = 0$. Except for the slight generalization on the coupling matrix Υ_i this analysis was performed in Ref. [48]. We perform the analysis at $T = 0$ and assume that the normal state is critical, i.e., we analyze the problem right at the GN-critical point, which corresponds to a critical value of the coupling constant $g_c \sim \omega_0 \Lambda^{-1/2}$ with upper momentum cut off Λ. In our analysis of the critical state the following expressions for Fourier transformations will be useful:

$$\begin{aligned} \int d^3x |x|^{-2a} e^{ix_\mu q^\mu} &= C_a |q|^{2a-3}, \\ \int d^3x x_\mu \gamma^\mu |x|^{-2a-1} e^{ix_\mu q^\mu} &= -iB_a q_\mu \gamma^\mu |q|^{2a-4}, \end{aligned} \tag{27}$$

where $C_a = \frac{2^{3-2a}\pi^{3/2}\Gamma(\frac{3}{2}-a)}{\Gamma(a)}$ and $B_a = \frac{C_{a-\frac{1}{2}}}{1-2a}$. The analogous expressions of the inverse transforms follow immediately.

For a critical system we make the power law ansatz

$$\begin{aligned} \Sigma(k) &= -A(i\omega - v\boldsymbol{k}\cdot\boldsymbol{\alpha})|k|^{-\eta_\psi}, \\ &= -iAk_\mu \gamma^\mu \gamma^0 |k|^{-\eta_\psi}, \end{aligned} \tag{28}$$

with amplitude $A > 0$ and exponent η_ψ. We determine the exponent from the coupled saddle point equations. For $\eta_\psi > 0$ the self-energy gives rise to a branch cut in the spectrum that renders quasiparticle excitations ill-defined, with life times and excitation energies of comparable magnitude, as seen in Fig. 2 for the normal state spectral function. In the infrared regime $\Sigma(k)$ dominates over the bare propagator and we obtain from the Dyson equation $G(k)^{-1} \approx -\Sigma(k)$ which yields

$$G(k) = -\frac{i}{A}\gamma^0 \frac{k_\mu \gamma^\mu}{|k|^{2-\eta_\psi}}. \tag{29}$$

Fourier transformation to coordinate space yields the result

$$G(x) = -\frac{B_{\frac{1}{2}(1-\eta_\psi)}}{(2\pi)^3 A}\gamma^0 \frac{\gamma^\mu x_\mu}{|x|^{3+\eta_\psi}}. \tag{30}$$

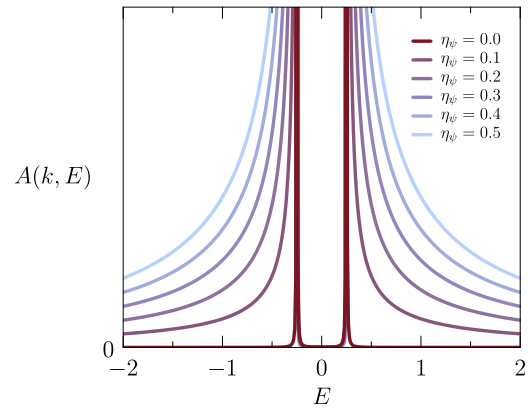

FIG. 2. Normal state single-particle spectral function $A(\boldsymbol{k}, E) = -\mathrm{Im}[\mathrm{Tr}G(\boldsymbol{k}, i\omega \to E + i0^+)]$ vs energy E with self-energy Eq. (28), showing the evolution from sharp quasiparticle peaks at vanishing η_ψ to a branch-cut behavior at larger η_ψ that show the absence of well-defined quasiparticles. We use amplitude $A = 1$, a wave vector $|\boldsymbol{k}| = 0.25$, and exponents $\eta_\psi \sim 0 - 0.5$.

For the bosonic propagator follows from Eq. (22)

$$\Pi(x) = 4g^2 \frac{B^2_{\frac{1-\eta_\psi}{2}}}{(2\pi)^6 A^2} \frac{c_{\mu\nu} x_\mu x_\nu}{|x|^{6+2\eta_\psi}}, \tag{31}$$

where $c_{\mu\nu} = \frac{1}{4}\mathrm{tr}(\Upsilon_i \gamma^0 \gamma^\mu \Upsilon_i \gamma^0 \gamma^\nu)$. For the four coupling matrices Υ_i of Eq. (6) that anticommute with the α_i follows that $c_{\mu\nu} = \delta_{\mu\nu}$. Returning to momentum space we separately analyze the zero momentum contribution and the dynamic part

$$\Pi(q) = \Pi(0) + \delta\Pi(q). \tag{32}$$

Being in a critical state it must hold that the renormalized boson frequency

$$\omega_r^2 = \omega_0^2 - \Pi(0), \tag{33}$$

vanishes at $T = 0$. We then obtain

$$\Pi(q) = \omega_0^2 - g^2 \frac{c_\Pi}{A^2} |q|^{1+2\eta_\psi} \tag{34}$$

with $c_\Pi = -4B^2_{\frac{1-\eta_\psi}{2}} C_{2+\eta_\psi}/(2\pi)^6$, which yields for the bosonic propagator

$$D(q) = \frac{A^2}{g^2 c_\Pi} \frac{1}{|q|^{1+2\eta_\psi}}. \tag{35}$$

Note that compared to the GN critical point in Eq. (2) the anomalous exponents of the bosonic and fermionic propagators are connected by $\eta_\phi = 1 - 2\eta_\psi$. The Fourier transform is $D(x) = \frac{A^2}{g^2} c_D |x|^{2\eta_\psi - 2}$ with $c_D = -\frac{(2\pi)^3 C_{\frac{1}{2}+\eta_\psi}}{4B^2_{\frac{1-\eta_\psi}{2}} C_{2+\eta_\psi}}$. This yields for the self-energy:

$$\Sigma(x) = -\frac{AM}{4N} \frac{C_{\frac{1}{2}+\eta_\psi}}{B_{\frac{1-\eta_\psi}{2}} C_{2+\eta_\psi}} |x|^{\eta_\psi - 5} \Upsilon_i \gamma^0 \gamma^\mu x_\mu \Upsilon_i, \tag{36}$$

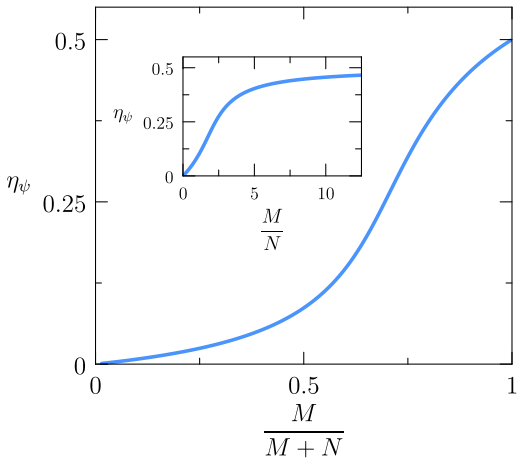

FIG. 3. Dependence of the anomalous exponent of the fermion spectrum on the ratio M/N of the bosonic and fermionic flavors, respectively (notice, as we consider four-component Dirac spinors, we have in total $4N$ fermion flavors). Crucially, the approach used here allows for a controlled analysis of η_ψ that is not parametrically small and reaches values up to $\eta_\psi = \frac{1}{2}$.

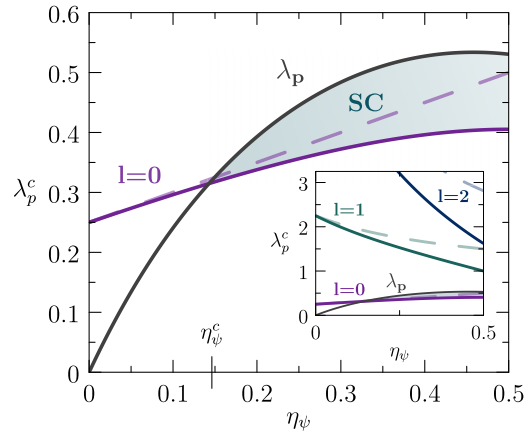

FIG. 4. Critical coupling constants λ_p^c for various angular momenta l for the exact solution (solid purple line) and approximation (dashed purple line) of the single components superconducting problem that occurs for the pairing interactions Υ_1, Υ_2, and Υ_4. The pairing interaction λ_p (black line) exceeds the critical value for pairing for states with angular momentum in space-time $l = 0$ and for $\eta_\psi > 0.14628$, yielding a superconducting state (SC). The inset shows λ_p and the critical coupling constants λ_p^c for higher angular momenta l.

which we Fourier transform to momentum space and finally obtain

$$\Sigma(k) = i\frac{AM}{4N}\frac{C_{\frac{1}{2}+\eta_\psi} B_{\frac{4+\eta_\psi}{2}}}{B_{\frac{1-\eta_\psi}{2}} C_{2+\eta_\psi}} |k|^{-\eta_\psi} k_\mu \Upsilon_i \gamma^0 \gamma^\mu \Upsilon_i. \tag{37}$$

This result must be equal to our original ansatz, Eq. (28), to ensure that it is a self-consistent solution. This is indeed the case if

$$\frac{M}{N} = -4\frac{B_{\frac{1-\eta_\psi}{2}} C_{2+\eta_\psi}}{C_{\frac{1}{2}+\eta_\psi} B_{\frac{4+\eta_\psi}{2}}} = 2\frac{(\eta_\psi - 3)(\eta_\psi - 1)\sin^2\left(\frac{\pi\eta_\psi}{2}\right)}{\eta_\psi(2\eta_\psi + 1)\cos(\pi\eta_\psi)}, \tag{38}$$

as well as

$$\gamma^\mu = \Upsilon_i \gamma^0 \gamma^\mu \Upsilon_i \gamma^0 \tag{39}$$

for $\mu = 0, 1, 2$. The first equation determines the exponent η_ψ. Analyzing the restrictions under which all Fourier integrals are convergent yields $0 < \eta_\psi < \frac{1}{2}$ for the exponent. In Fig. 3 we show η_ψ as function of the ratio M/N. It holds that $\eta_\psi \to 0$ as M/N goes to zero and $\eta_\psi \to 1/2$ in the opposite limit, $M/N \to \infty$. For $M = N$ follows $\eta_\psi \approx 0.08658$. As for the second condition, Eq. (39), on the coupling matrices, one easily finds that it is obeyed precisely for the four Υ_i listed in Eq. (6). Hence, Eq. (28) is a consistent solution for the normal state energy with η_ψ given by Eq. (38).

III. SUPERCONDUCTIVITY AT THE GROSS-NEVEU CRITICAL POINT

A. Linearized gap equation

In order to identify the leading superconducting instabilities we solve the saddle point Eq. (21) with the anomalous propagator evaluated to linear order in Φ:

$$\begin{aligned} F(p) &= -G(p)\Phi(p)u_T^\dagger G^T(-p)u_T, \\ &= -\frac{p_\mu p_\nu}{A^2|p|^{4-2\eta_\psi}} \gamma^0\gamma^\mu\Phi(p)\gamma^\nu\gamma^0. \end{aligned} \tag{40}$$

In the last step we used the critical normal state solution for $G(p)$, discussed in the previous section. If we furthermore use the corresponding power-law result for the boson propagator, the linearized version of Eq. (21) becomes

$$\Phi(k) = \lambda_p \tau_i \int \frac{d^3p}{4\pi} \frac{p_\mu p_\nu \Upsilon_i \gamma^0 \gamma^\mu \Phi(p) \gamma^\nu \gamma^0 \Upsilon_i}{|p|^{4-2\eta_\psi}|k-p|^{1+2\eta_\psi}}, \tag{41}$$

where we introduced the coupling constant of the pairing problem

$$\lambda_p(\eta_\psi) = \frac{1}{2\pi^2 c_\Pi}\frac{M}{N}. \tag{42}$$

Using Eq. (38) for M/N and c_Π as given in the text below Eq. (34), it follows that this coupling constant is fully determined by the anomalous exponent η_ψ of the fermions; in particular it is independent of the amplitude A of the fermionic propagator and the value of the coupling constant g. For small η_ψ it holds $\lambda_p \approx 3\eta_\psi(1 - \frac{7}{3}\eta_\psi \cdots)$ while $\lambda_p(\eta_\psi \to \frac{1}{2}) \to \frac{5}{3\pi}$. In Fig. 4 we show the dependence of λ_p on η_ψ for $0 < \eta_\psi < \frac{1}{2}$, i.e., the entire regime of relevance.

Equation (41) is the linearized gap equation of pairing in quantum critical Dirac fluids. It determines the momentum and frequency dependence as well as the spinor structure of the superconducting state. Both are closely entangled, a property that will be crucial in our subsequent solution of this integral equation. While formally our analysis is performed at $T = 0$, finite temperatures can easily be reintroduced as one converts the frequency integration to a Matsubara summation,

or, approximately, by introducing a lower cut off $\sim T$ of the frequency integral.

In order to analyze the pairing state we first focus on its structure in spinor space. Since $\Phi(k)$ transforms properly under symmetry operations, it is natural to expand it in terms of the basis matrices of Eq. (18):

$$\Phi(k) = \sum_{rJ} \chi_J^r(k)\Gamma_J^r, \tag{43}$$

such that

$$\chi_J^r(k) = \lambda_p \tau_i \sum_{r'J'} \int \frac{d^3p}{4\pi} \frac{L_{JJ'}^{rr'}(p)\chi_{J'}^{r'}(p)}{|p|^{2-2\eta_\psi}|k-p|^{1+2\eta_\psi}}, \tag{44}$$

with

$$L_{JJ'}^{rr'}(p) = \frac{p_\mu p_\nu}{4p^2}\mathrm{tr}\left(\Upsilon_i\gamma^0\gamma^\mu\Gamma_J^r\gamma^\nu\gamma^0\Upsilon_i\Gamma_{J'}^{r'}\right). \tag{45}$$

Here, the summation is over μ and ν, while no summation over i, i.e., over the choice of the coupling matrix Υ_i, is implied. To keep the number of indices manageable we do not indicate explicitly that $L_{JJ'}^{rr'}(p)$ depends on i. It holds for all four Υ_i that $L_{JJ'}^{rr'}(p)$ is diagonal w.r.t. S, V, T, A, and P that stand for scalar, vector, (antisymmetric) tensor, axial vector, and pseudoscalar, respectively, i.e.,

$$L_{JJ'}^{rr'}(p) = l_J^{rr'}(p)\delta_{J,J'}. \tag{46}$$

The eigenvalues l_J of the matrices $l_J^{rr'}(p)$ are momentum independent and ± 1. The eigenvectors only depend on the direction of $p = (\omega, \boldsymbol{p})$ and not on its magnitude, which we denote as $P = |p|$.

Let us analyze these matrices for the distinct pairing symmetries, i.e., for different J. If $J = S$ it holds for all four pairing interactions Υ_i

$$l_S = 1. \tag{47}$$

If the pairing state is of a vector nature, the pairing matrix $l_V^{rr'}(p)$ is a 4×4 matrix

$$l_V = p_i \begin{pmatrix} Q_{\mu\nu} & 0 \\ 0 & b_i \end{pmatrix}, \tag{48}$$

with 3×3 block $Q_{\mu\nu} = \frac{2q^\mu q^\nu}{q^2} - \delta^{\mu\nu}$ and $2+1$-dimensional momenta q^μ as well as a 1×1 block. We recall that p_i is the parity of the boson and $b_i = \pm 1$ determines whether γ^5 commutes or anticommutes with the coupling matrix Υ_i. Obviously the result depends on the behavior of the pairing matrix Υ_i. The expression for the 6×6 matrix l_T, that describes antisymmetric tensor matrices, is rather lengthy. As we will see, we will not need it in our subsequent analysis. For pairing states with axial vector character it holds $l_A = b_i l_V$, while for pseudoscalars it holds that

$$l_P = b_i. \tag{49}$$

These results are summarized in Table I.

B. Pairing symmetry and Pauli principle

Before we solve the linearized gap equation further, we summarize the implications of the Pauli principle for the pairing amplitudes $\chi_J^r(k)$. If we consider a pairing expectation value $\Delta_{ab}(k) \sim \langle \psi_a(k)\psi_b(-k)\rangle$, fermionic anticommutation yields $\Delta(k) = -\Delta^T(-k)$, which corresponds with Eq. (15) to

$$\Phi(k) = -u_T^* \Phi^T(-k) u_T. \tag{50}$$

If we now insert the expansion of Eq. (43) into Eq. (50) and use the orthogonality of the Γ_J^r it follows that

$$\chi_{rJ}(k) = \tau_J \chi_{rJ}(-k), \tag{51}$$

where τ_J is the parity of Γ_J^r under time reversal, i.e., $u_T^\dagger \Gamma_J^{rT} u_T = \tau_J \Gamma_J^r$ with $\tau_J = \pm 1$, independent on r. To derive Eq. (51) we used $u_T^* = -u_T^\dagger$ valid for $\mathcal{T}^2 = -1$. Thus, for pairing states with time-reversal (TR)-even spinor structure, $\chi_{rJ}(k)$ is an even function of $k = (\omega, \boldsymbol{k})$, while it is odd if the pairing state has a spinor structure that is odd under TR. Since $\tau_S = \tau_V = \tau_P = 1$ and $\tau_T = \tau_A = -1$, it follows for the Pauli condition

$$\begin{aligned} \chi_S(k) &= \chi_S(-k), \\ \chi_V(k) &= \chi_V(-k), \\ \chi_T(k) &= -\chi_T(-k), \\ \chi_A(k) &= -\chi_A(-k), \\ \chi_P(k) &= \chi_P(-k). \end{aligned} \tag{52}$$

This is analogous to singlet states being even and triplet states odd under $k \to -k$ for single orbital pairing [73]. Below we find that in an expansion in spherical harmonics with respect to the three-dimensional vector k, only pairing states with angular momentum $l = 0$ occur. This immediately excludes $\chi_T(k)$ and $\chi_A(k)$ which only contain odd l.

C. Gap equation in spherical harmonics

To solve the linearized gap equation, where the spinor structure and the momentum dependence are strongly coupled, we expand the pairing wave function and interaction in spherical harmonics:

$$\begin{aligned} \chi_J^r(p) &= \sum_{lm} \varphi_{lm}^r(P) Y_{lm}(\Omega_p), \\ l_J^{rr'}(\Omega_p) &= \sum_{lm} \Lambda_{lm}^{rr'} Y_{lm}(\Omega_q), \\ \frac{1}{|k-p|^{1+2\eta_\psi}} &= \sum_{l,m} \frac{4\pi z_l(P/K) Y_{lm}(\Omega_k) Y_{lm}^*(\Omega_p)}{(K^2+P^2)^{1/2+\eta_\psi}}. \end{aligned} \tag{53}$$

We recall that $P = |p|$ and $K = |k|$ stand for the magnitudes of the three vectors. In Eq. (53) we dropped, for simplicity, the index J in φ_{lm}^r and $\Lambda_{l_2 m_2}^{rr'}$ on the right-hand side, and used

$$z_l(s) = \frac{1}{2}\int_{-1}^{1} dx P_l(x)\left(1 - \frac{2sx}{1+s^2}\right)^{-1/2-\eta_\psi}, \tag{54}$$

with Legendre polynomial $P_l(x)$. It holds $z_l(s) = z_l(s^{-1})$. Below we will also employ the asymptotic behavior

$$z_l(s) = z_l^0 \begin{cases} s^l & \text{if} \quad s \ll 1 \\ s^{-l} & \text{if} \quad s \gg 1 \end{cases}, \tag{55}$$

with $z_l^0 = \frac{\prod_{l'=0}^{l-1}(2l'+1+2\eta_\psi)}{(2l+1)!!}$, implying $z_{l=0}^0 = 1$.

This expansion then yields for the gap equation

$$\varphi^{r}_{lm}(K) = \lambda_{\rm p}\tau_i \sum_{r'l'm'} \int_0^\infty dP \frac{M^{rr'}_{lm,l'm'} z_l(P/K)}{(K^2+P^2)^{1/2+\eta_\psi} P^{-2\eta_\psi}} \varphi^{r'}_{l'm'}(P), \tag{56}$$

where we only have a one-dimensional integration over the magnitude $P = \sqrt{\omega^2 + \boldsymbol{p}^2}$ left. We introduced

$$M^{rr'}_{lm,l'm'} = \sum_{l''m''} \Lambda^{rr'}_{l''m''} T^{lm}_{l''m'',l'm'}, \tag{57}$$

that describes the angular momentum transferred by the interaction. Analyzing this transferred momentum, only $l''=0$ and $l''=2$ occur since $l^{rr'}_J(\Omega_p)$ only contains constant terms or terms that transform like a quadrupole $p_\mu p_\nu/p^2$ in space time, see e.g., $l^{r,r'}_V$ of Eq. (48). Finally, $T^{lm}_{l''m'',l'm'}$ vanishes unless $|l''-l'| \leqslant l \leqslant l''+l'$ when it is expressed in terms of Clebsch-Gordon coefficients:

$$T^{lm}_{l''m'',l'm'} = \sqrt{\frac{(2l'+1)(2l''+1)}{4\pi(2l+1)}} \langle l''0l'0 \mid l0\rangle \times \langle l''m''l'm' \mid lm\rangle. \tag{58}$$

Next we solve this pairing problem for the different pairing states.

1. Scalar and pseudoscalar, and one-component vector pairing states

The situation is particularly simple for pairing in the scalar and pseudoscalar channel $J=S$ and P or for the one-dimensional block of the vector channel V, where the indices r, r' only take one value; and hence the matrix (or matrix block) obeys $l^{rr'}_J = \pm 1$. In this case it holds that

$$M_{lm,l'm'} = \delta_{l,l'}\delta_{m,m'}. \tag{59}$$

Then it follows for the linearized gap equation that the integral equation

$$\varphi_{lm}(K) = l_J \tau_i \lambda_{\rm p} \int_0^\infty dP \frac{z_l(P/K)\varphi_{lm}(P)}{(K^2+P^2)^{1/2+\eta_\psi} P^{-2\eta_\psi}}. \tag{60}$$

This integral equation is formally very similar to the one that occurs in compressible quantum critical systems, often referred to as the "γ model" [74–82], with exponent $\gamma = 1+2\eta_\psi$ (i.e., $1<\gamma<2$). Notice, in compressible systems the variable K corresponds to the fermionic frequency, while it is the Lorentz-invariant magnitude $K=\sqrt{\omega^2+\boldsymbol{k}^2}$ in our problem. The common feature of both problems is the highly nonlocal pairing interaction in K.

Nontrivial solutions of Eq. (60) require $\tau_i l_J = +1$, i.e., for TR even bosons $l_J=+1$ matters while eigenvalues $l_J=-1$ are important for TR odd bosons. As one can deduce from Table I, this is the case for $\Upsilon_1=\gamma^0$ if $J=S$, for $\Upsilon_2 = i\gamma^0\gamma^3$ if $J=V$ as long as we consider the one-dimensional block -1, and for $\Upsilon_4 = i\gamma^0\gamma^5$ with $J=P$. These three states are marked with green color in the table. In what follows we consider those cases and set $\tau_i l_J = +1$.

We start our analysis by performing an approximate solution of this integral equation. Following Refs. [55,76,82,83] we transform the integral equation into a differential equation with appropriate boundary conditions. This is, as we will see, even quantitatively accurate for η_ψ not too small. In addition, it will provide us with the intuition to solve the problem more accurately. We split in Eq. (60) the contributions for $P<K$ and $P>K$ and treat them in the limits $P \ll K$ and $P \gg K$. Using Eq. (55) this leads to

$$\varphi_{lm}(K) = \lambda_{\rm p} z^0_l \left(\int_T^K \frac{dP\varphi_{lm}(P)}{K^{l+1+2\eta_\psi} P^{-l-2\eta_\psi}} + \int_K^\Lambda \frac{dPK^l\varphi_{lm}(P)}{P^{1+l}} \right). \tag{61}$$

Here we introduced the temperature, T, as a lower cut off and added an upper cut off Λ above which the power-law behavior ceases to be correct. In this form, the equation can easily be transformed into a differential equation. First we find

$$\partial_K K^{l+1+2\eta_\psi}\varphi_{lm}(K) = \lambda_{\rm p} z^0_l (2(l+\eta_\psi)+1) \times \int_K^\Lambda dP \frac{K^{2(l+\eta_\psi)}}{P^{1+l}} \varphi_{lm}(P), \tag{62}$$

which leads to the second-order differential equation

$$\partial_K K^{-2(l+\eta_\psi)} \partial_K K^{l+1+2\eta_\psi} \varphi_{lm}(K) = -\lambda_{\rm p}(2(l+\eta_\psi)+1) z^0_l \frac{\varphi_{lm}(K)}{K^{1+l}}. \tag{63}$$

From Eq. (63) also follow the UV and infrared (IR) boundary conditions $\partial_K K^{l+1+2\eta_\psi}\varphi_{lm}(K)|_{K=\Lambda} = 0$ and $K\partial_K\varphi_{lm}(K)|_{K=T} = l\varphi_{lm}(T)$, respectively. Finally, we use logarithmic variables

$$\varphi_{lm}(K) = K^{-1/2-\eta_\psi} f_{lm}\left(\log\frac{K}{\Lambda}\right), \tag{64}$$

and the above differential equation takes a particularly simple form of a classical harmonic oscillator problem:

$$\frac{d^2 f_{lm}(x)}{dx^2} = v_l f_{lm}(x), \tag{65}$$

with $v_l = \frac{1}{4}(2(l+\eta_\psi)+1)^2 - (2(l+\eta_\psi)+1)\lambda_{\rm p} z^0_l$. The boundary conditions are $\partial_x f_{lm}(x)|_{x=0} = -\frac{2(l+\eta_\psi)+1}{2} f_{lm}(0)$ in the UV and $\partial_x f_{lm}(x)|_{x=x_T} = \frac{2(l+\eta_\psi)+1}{2} f_{lm}(x_T)$ with $x_T = \log(\Lambda/T)$ in the IR. If $v_l>0$ one cannot simultaneously fulfill both boundary conditions. This changes once v_l becomes negative and the solutions of the differential equation become oscillatory with $f_{lm}(x) \sim e^{\pm i\sqrt{-v_l}x}$. For $v_l<0$, the boundary conditions then determine the transition temperature as

$$T_c = \Lambda \exp\left(-\frac{1}{\sqrt{|v_l|}} \left(\pi - \arctan \frac{4(1+2\eta_\psi)\sqrt{|v_l|}}{(1+2\eta_\psi)^2 - 4|v_l|} \right) \right), \tag{66}$$

which we plot for $l=0$ in Fig. 1. Near the onset of superconductivity this expression simplifies to

$$T_c = \Lambda \exp\left(-\frac{D}{\sqrt{\lambda_{\rm p} - \lambda^c_{\rm p}}} \right), \tag{67}$$

where $D = \frac{\pi}{\sqrt{1+2\eta_\psi}}$. The coupling constant λ_p of Eq. (42) must therefore be larger than the critical value $\lambda_p^c = \frac{1}{4z_l^0}(2(l + \eta_\psi) + 1)$, determined from the condition that ν_l vanishes. Hence a superconducting ground state only emerges if λ_p of Eq. (42) is larger than λ_p^c. The behavior of Eq. (67) for the transition temperature is common to a number of quantum-critical pairing states [54,55,74], and generally associated with the spontaneous breaking of conformal symmetry [84].

Returning from logarithmic variables to our usual momenta yields

$$\varphi_{lm}(P) \propto P^{-\frac{1}{2}-\eta_\psi \pm i\delta}, \tag{68}$$

where the exponent $\delta = \sqrt{|\nu_l|}$ vanishes for $\lambda_p \to \lambda_p^c$ from above. It turns out that this is indeed the correct solution of the full integral Eq. (60), provided the following condition is met:

$$1 = 2\lambda_p \int_0^1 ds \frac{z_l(s)\cos(\delta \log s)}{(s^2+1)^{\frac{1}{2}+\eta_\psi} s^{-\eta_\psi}}. \tag{69}$$

The critical coupling constant for the onset of pairing with angular momentum l is obtained if one considers $\delta \to 0$

$$\lambda_{p,l}^c = \frac{1}{2}\left(\int_0^1 ds \frac{z_l(s)}{(s^2+1)^{\frac{1}{2}+\eta_\psi} s^{-\eta_\psi}}\right)^{-1}; \tag{70}$$

the ground state is superconducting if $\lambda_p > \lambda_{p,l}^c$.

In Fig. 4 we plot $\lambda_{p,l}^c$ for the various angular momentum states l. Clearly the leading instability is the one with $l = 0$, while other pairing states require significantly larger coupling constants. We also compare the critical coupling constant with the approximate result that follows from the analysis of the differential equation. For exponents η_ψ not too far from zero the agreement is very good. In the figure we also show λ_p of Eq. (42). We see that only $l = 0$ instabilities are allowed and require $\eta_\psi > \eta_\psi^c$, with η_ψ^c of Eq. (3). For all angular momenta $l \geqslant 1$, the pairing strength is not strong enough to induce higher angular-momentum pairing. Hence, if the anomalous dimension of the fermions is sufficiently large, the ground state of the problem is superconducting and the pairing wave function is isotropic as function of the three momentum ($l = 0$). In particular this implies that the pairing state is of even frequency. Thus, for $\Upsilon_1 = \gamma^0$ the pairing state is

$$\Phi(P) \sim P^{-\frac{1}{2}-\eta_\psi \pm i\delta} 1, \tag{71}$$

for $\Upsilon_2 = i\gamma^0\gamma^3$ it holds that

$$\Phi(P) \sim P^{-\frac{1}{2}-\eta_\psi \pm i\delta} \gamma^3, \tag{72}$$

while for $\Upsilon_4 = i\gamma^0\gamma^5$ it holds that

$$\Phi(P) \sim P^{-\frac{1}{2}-\eta_\psi \pm i\delta} \gamma^5. \tag{73}$$

In Fig. 5 we show the spectral function on the real frequency axis in the superconducting state and near the onset of pairing that results from this anomalous pairing state. Clearly, states at the Dirac point are gapped by pairing, i.e., the GN gap due to condensation of the critical boson is preempted by the onset of superconductivity.

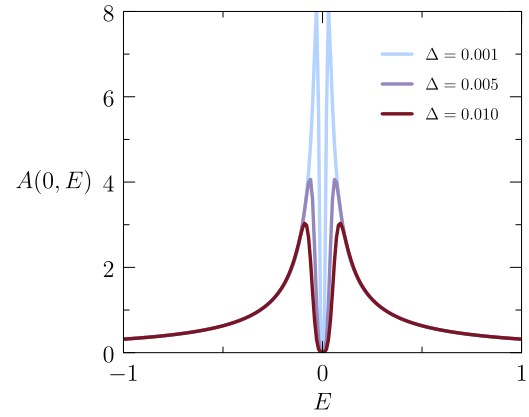

FIG. 5. Single-particle spectral function $A(\boldsymbol{k}, E) = -\mathrm{Im}[\mathrm{Tr}G(\boldsymbol{k}, i\omega \to E + i0^+)]$ vs energy E, evaluated at $\boldsymbol{k} = \boldsymbol{0}$ (Dirac point) for the case of S pairing with diagonal self-energy Eq. (28) pairing self-energy $\Phi(\boldsymbol{k}, \omega) = \Delta(\boldsymbol{k}^2 + \omega^2)^{-\frac{1}{4}(1+2\eta_\psi)}$. For this plot we chose amplitude $A = 1$, exponent $\eta_\psi = 0.2$, pairing amplitude $\Delta = 0.001$ (light blue), $\Delta = 0.005$ (light purple), and $\Delta = 0.01$ (dark purple), showing that the onset of pairing rapidly suppresses the spectral function peak while also introducing a gap at the Fermi level.

2. Vector, tensor, and axial vector pairing states

In this section we analyze pairing instabilities for the situation where $l_f^{rr'}(p)$ describes coupling in a higher-dimensional state of pairing states and is no longer a 1×1 matrix. This is important for the pairing interaction $\Upsilon_3 = i\gamma^1\gamma^2$, where, according to Table I the 3×3 block Q enters as the only option to yield an attractive interaction.

To analyze these multicomponent pairing states we need to use the expansion of $l_f^{rr'}(p)$ given in Eq. (53). In analogy to the previous section, we first analyze the solution by approximately transforming the integral equation into a differential equation. With

$$\varphi_{lm}^r(K) = K^{-\frac{1}{2}-\eta_\psi} f_{lm}^r(\log K), \tag{74}$$

it follows that

$$\frac{d^2 f_{lm}^r(x)}{dx^2} = \sum_{r'l'm'} V_{lm,l'm'}^{rr'} f_{l'm'}^{r'}(x), \tag{75}$$

where we defined

$$V_{lm,l'm'}^{rr'} = \frac{(2(l+\eta_\psi)+1)^2}{4}\left(\delta_{rr'}\delta_{ll'}\delta_{mm'} - \lambda_p U_{lm,l'm'}^{(0)rr'}\right), \tag{76}$$

with

$$U_{lm,l'm'}^{(0)rr'} = \frac{4\tau_i z_l^0}{(2(l+\eta_\psi)+1)} M_{lm,l'm'}^{rr'}. \tag{77}$$

Pairing corresponds to the smallest eigenvalue of V crossing zero, i.e., the largest eigenvalue of $U^{(0)}$ reaching $1/\lambda_p$. The result for the 3×3 block $l_V = Q$, marked in red in Table I, is shown in Fig. 6. We find that the pairing strength λ_p never crosses the critical value.

To check this result, we solve the linearized gap equation more carefully and find that the ansatz

$$\varphi_{lm}^r(P) = A_{lm}^r P^{-\frac{1}{2}-\eta_\psi \pm i\beta}, \tag{78}$$

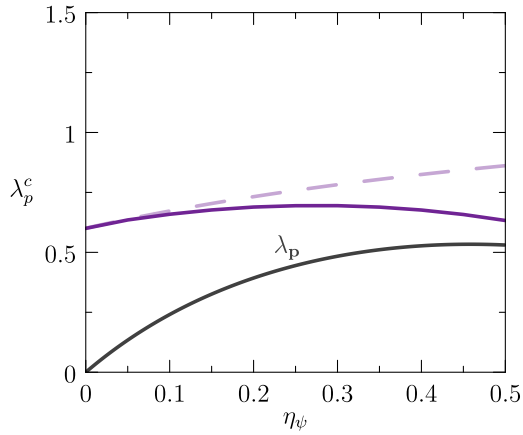

FIG. 6. Same as Fig. 4, but for a pairing interaction Υ_3 that leads to the 3×3 matrix Q which occurs in the vector component l_V. The dashed-purple line corresponds to the threshold coupling obtained from the approximate solution of the differential equation, while the solid-purple line corresponds to the full solution. For this interaction the pairing interaction λ_p (shown as black line) is always smaller than the threshold coupling for superconductivity λ_p^c, i.e. no superconductivity emerges.

solves the integral equation, provided the largest eigenvalue of the matrix

$$U^{rr'}_{lm,l'm'} = 2\tau_i M^{rr'}_{lm,l'm'} \int_0^1 ds \frac{z_l(s)}{(s^2+1)^{\frac{1}{2}+\eta_\psi} s^{-\eta_\psi}} \tag{79}$$

equals $\lambda_{\rm p}^{-1}$. In Fig. 6 we show for the 3×3 matrix Q that enters in the vector component l_V the approximate solution from the differential equation as well as the full solution using U of Eq. (79) as function of the anomalous exponent η_ψ. We find that the condition $\lambda_{\rm p} > \lambda_{\rm p}^c$ cannot be fulfilled, i.e., critical fluctuations of a boson coupled via $\Upsilon_3 = i\gamma^1\gamma^2$ will not give rise to a stable superconducting state. The complexity of the multicomponent pairing state leads to an enhanced threshold coupling, which is always larger than λ_p, including for $l = 0$.

D. Algebraic conditions for pairing

Our results for pairing can be expressed very efficiently as algebraic conditions on the matrices Γ^r_J that, according to Eq. (43), govern the spinor structure of the pairing state. To this end, we generalize from four-component to n_γ-component spinors and to bosons with m_ϕ degenerate components, described by Υ_i ($i = 1, \ldots, m_\phi$), all sharing the same parity under time reversal τ. In this framework, the matrix $L^{rr'}_{JJ'}(p)$ of Eq. (45) takes the form

$$L^{rr'}_{JJ'}(p) = \frac{p_\mu p_\nu}{m_\phi n_\gamma p^2} \sum_{i=1}^{m_\phi} \mathrm{tr}\left(\Upsilon_i \gamma^0 \gamma^\mu \Gamma^r_J \gamma^\nu \gamma^0 \Upsilon_i \Gamma^{r'}_{J'}\right). \tag{80}$$

It is now an $n_\gamma^2 \times n_\gamma^2$ matrix. The analysis of the linearized pairing problem implies that superconductivity becomes possible if $L(p)$ has one-dimensional irreducible sub-blocks with $(L)_{\text{sub block}} = \tau$. One can easily show that this condition is fulfilled for the (r, J) that obey

$$\left[\Gamma^r_J, \alpha_i\right] = 0 \ \text{ for } i = 1, 2, \tag{81}$$

and

$$\Gamma^r_J \Upsilon_i = \tau \Upsilon_i \Gamma^r_J \ \text{ for } i = 1 \cdots m_\phi. \tag{82}$$

Hence, for $\tau = -1$ it holds that the pairing matrix and the Υ_i anticommute $\{\Gamma^r_J, \Upsilon_i\} = 0$ while they commute for $\tau = +1$, $[\Gamma^r_J, \Upsilon_i] = 0$. An allowed pairing state must also obey the Pauli principle, which for an angular-momentum $l = 0$ state implies

$$(\Gamma_J u_T)^T = -\Gamma_J u_T. \tag{83}$$

The three algebraic conditions Eqs. (81), (82), and (83) for Γ^r_J allow for an easy determination of superconductivity in a generic Dirac problem coupled to arbitrary critical bosons. Interestingly, the second condition, Eq. (82), was recently obtained in the study of the leading pairing instability of twisted bilayer graphene in the extreme flat-band limit [85] and for doped Dirac systems [86,87], i.e., not in the Dirac regime or at neutrality, suggesting that it may in fact be of more general relevance. This point will be elaborated further in Ref. [70].

E. Absence of pairing for two-component Dirac spinors

It is instructive to apply our formalism and analyze for the possibility of pairing near the GN-critical point for a two-component Dirac spinor, i.e., the simplest Dirac theory in $2+1$ dimensions. To this end we make, without restrictions, the choice

$$\alpha_1 = \sigma_1, \ \alpha_2 = \sigma_2, \tag{84}$$

coupled to the only mass-generating term with

$$\Upsilon = \sigma_3. \tag{85}$$

The σ_i are the usual Pauli matrices. If the fermions are spinless the unitary component of time reversal is $u_T = \sigma_0$ (the unit matrix) and Υ is time-reversal even, i.e., $\tau = 1$. If σ_i stand for spin, then $u_T = i\sigma^y$ and Υ is time-reversal odd with $\tau = -1$. The complete set of Hermitian 2×2 matrices is given by $\Gamma_J = \sigma_J$ with $J = 0 \cdots 3$. This immediately allows us to determine the matrix

$$L = \begin{pmatrix} l_S & 0 \\ 0 & l_V \end{pmatrix}, \tag{86}$$

where $l_S = 1$ and $l_V = -Q$ with the 3×3 matrix used earlier. As before, l_V will not induce pairing. The pairing wave function in the l_S channel is $\Phi(k) = \chi(k)\sigma_0$. It seems that a TR even critical boson might cause superconductivity since $\tau l_S = +1$. However, due to $u_T = \sigma_0$ it follows that $\Delta(k) = \chi(k)\sigma_0$ and the function $\chi(k)$ must be odd in k to comply with Pauli principle. Even for the smallest angular momentum $l = 1$ the threshold value for the pairing interaction is too large. The Pauli principle would be consistent with $l = 0$ for spin-full fermions where $\Delta(k) = \chi(k) i\sigma_2$ corresponds to a singlet state. However, in this case $\tau l_S = -1$ and the interaction is repulsive. Hence, no superconductivity emerges in a two-component Dirac spinor.

We can easily come to the same conclusion using the three algebraic conditions (81), (82), and (83): Given our choice for α_1 and α_2, the only 2×2 matrix that commutes with both, i.e., that is a candidate for Γ_J, is σ_0. σ_0 does not anticommute with Υ, i.e. there is no attractive coupling for TR odd bosons.

It commutes with Υ and could serve as pairing state for a TR even boson. However, in this case it holds that $u_T = \sigma_0$ and $\sigma_0 u_T$ is not antisymmetric. Hence, we arrive at the same conclusion that no pairing state is allowed. More complex spinor structures are necessary for pairing near the GN critical point to emerge.

F. Superconducting order-parameter fluctuations

The solution of the pairing problem yields an instability temperature T_c. Within the large-N approach used here, superconducting order-parameter fluctuation are suppressed and and T_c corresponds to the actual phase transition temperature. For any finite N order-parameter fluctuations are of course important and ultimately give rise to a Berezinskii-Kosterlitz-Thouless (BKT) transition [88–90]. Furthermore, the pairing state we find exhibits off-diagonal long-range order and therefore displays a Meissner effect —understood in the appropriate sense for a two-dimensional superconductor —as well as flux quantization. In what follows we show that superconducting fluctuations will give rise to corrections to T_c of order unity, but that ultimately the BKT transition temperature remains finite and is of the order of magnitude of T_c.

To analyze BKT physics we need to determine the phase stiffness of the problem. The stiffness then determines the behavior of the two-dimensional classical problem at finite temperature with XY action

$$S_{\mathrm{XY}} = \frac{\rho_s^{(0)}}{2} \int d^2x (\nabla\theta - 2e\boldsymbol{A})^2, \tag{87}$$

where θ is the phase of the superconducting order parameter and $\boldsymbol{A}$ the electromagnetic vector potential. Order-parameter fluctuations renormalize $\rho_s^{(0)} \to \rho_s$ and the BKT transition temperature follows from the celebrated condition [89,90]

$$\rho_s(T_{\mathrm{BKT}}) = \frac{2}{\pi} T_{\mathrm{BKT}}. \tag{88}$$

The determination of the superfluid stiffness is a nontrivial analysis, which requires the determination of current vertex corrections; a consequence of the strong momentum dependence of the single-particle self-energy. This is rather different from the usual analysis in Eliashberg-type theories with momentum-independent self energies; for a detailed discussion see Ref. [91]. Qualitative understanding can, however, be obtained using the Ferrell-Glover-Tinkham (FGT) sum rule of the real part $\sigma'(\omega)$ of the optical conductivity [92,93]:

$$\frac{\omega_p^2}{4} = \int_{-\infty}^{\infty} d\omega \sigma'(\omega), \tag{89}$$

with plasma frequency ω_p. For a Dirac particle with upper cut off Λ the sum rule becomes [94]

$$\int_{-\Lambda}^{\Lambda} d\omega \sigma'(\omega) = \frac{N}{4}\Lambda. \tag{90}$$

In the superconducting state it holds for the real part of the optical conductivity

$$\sigma'_{\mathrm{sc}}(\omega) = \pi e^2 \rho_s \delta(\omega) + \tilde{\sigma}_{\mathrm{ns}}(\omega), \tag{91}$$

where $\tilde{\sigma}_{\mathrm{ns}}(\omega)$ essentially equals the normal state conductivity for $|\omega| > T$ and is due to interband transitions. We expect it to vanish at low frequencies, below the pairing gap Δ. We further expect that this gap is parametrically determined by the mean-field transition temperature: $\Delta \sim T_c$, where the coefficient is of the order of unity but typically somewhat larger. The spectral weight of the optical conductivity below $\omega < \Delta$ in the normal state is transferred into a δ-function in the superconducting state, as illustrated in Fig. 7. In the normal state, hydrodynamic arguments [95,96] fix the conductivity for $\omega < T$ to a Drude contribution:

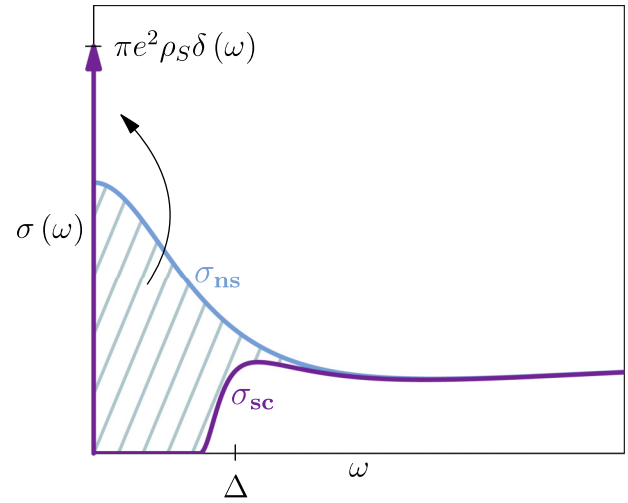

FIG. 7. The transfer of spectral weight in the optical conductivity from the normal state behavior (light blue) to the superconducting state (dark purple) determine the superfluid stiffness ρ_S and is determined by the gap energy scale Δ and the normal state DC conductivity σ_0. For the latter we expect $\sigma_0 \sim Ne^2/\hbar$ which implies $\rho_S \sim N\Delta$, i.e., phase fluctuations are important at finite N and change the transition temperature compared to its value obtained from the large-N theory.

$$\sigma'_{\mathrm{ns}}(\omega) = \frac{\sigma_0}{1 + (\omega\tau)^2} + \tilde{\sigma}_{\mathrm{ns}}(\omega). \tag{92}$$

Then follows from the FGT sum rule for $\Delta\tau \approx 1$ that

$$\pi \frac{e^2}{\hbar} \rho_s \approx \sigma_0 \Delta. \tag{93}$$

In the usual weakly disordered Fermi liquid it holds that $\sigma_0 = \frac{\omega_p^2}{4\pi}\tau$ and we obtain for the stiffness in the superconducting state $\rho_s = \frac{n}{m}\frac{\pi}{4}\tau\Delta$ with $\omega_p^2 = \pi\frac{e^2}{\hbar}\frac{n}{m}$. For $\frac{n}{m}\frac{\pi}{4}\tau \approx E_F\tau \gg 1$ the stiffness, albeit reduced from its clean limit, is large compared to Δ and phase fluctuations are relevant only in a very narrow regime near T_c. Then T_{BKT} is smaller than, but very close to T_c [90]. In our problem we expect for the scattering rate at a critical point $\tau^{-1} = \alpha^* T$, with fixed point value of the interaction α^* along with the conductivity

$$\sigma_0 = N\zeta_* \frac{e^2}{h}, \tag{94}$$

where ζ_* should be a dimensionless number of order unity. This implies

$$\rho_s = N\zeta_* \frac{\Delta}{2\pi^2}. \tag{95}$$

At large N the stiffness is obviously large and there are no phase fluctuations. Considering $N = 1$ follows that $\rho_s \sim \Delta$

and phase fluctuations are strong near the transition temperature. Nevertheless, $(T_c - T_{\rm BKT})/T_{\rm BKT}$ of order unity since the stiffness scale is set by T_c. Hence, ultimately $T_{\rm BKT}$ should be of the same order as T_c. The stiffness at $T = 0$ can be understood in a similar way. Although the Drude peak is now absent, a nearly frequency-independent contribution to the optical conductivity from interband transitions persists down to the lowest frequencies and is again expected to be of order Ne^2/h. In other words, the stiffness is set by the zero-temperature gap. We therefore expect superconductivity to remain stable at sufficiently low temperatures, even for finite N.

IV. SUMMARY

In summary, we analyzed the possibility of superconductivity due to critical fluctuations at the Gross-Neveu critical point for two-dimensional massless Dirac fermions at neutrality, coupled to a bosonic mode by Yukawa coupling. For the bosonic mode we analyzed the four options that induce, upon bose condensation an isotropic gap in the fermion spectrum, see Eq. (6). In its normal state, the theory is identical to the one developed by Kim *et al.* [48] and yields anomalous dimensions η_ψ and η_ϕ for the Dirac fermions and critical bosons of the problem. Importantly, one then finds values for η_ψ that are not parametrically small, in distinction to the usual expansions in $1/N$ (with fermion flavor N) or in $\epsilon = 3 - d$. We then generalized the approach of Ref. [48] to the superconducting state and analyzed the linearized gap equation of the pairing problem. We find that superconductivity emerges once the anomalous fermion dimension exceeds a critical threshold. Strikingly, our analysis shows that superconductivity is absent in the regime of well-defined quasiparticles, but appears when the quasiparticles become ill-defined. We considered four distinct pairing interactions and found that superconductivity emerges in three out of the four cases. We further list easy-to-analyze algebraic conditions [Eqs. (81), (82), and (83)] that allow one to determine superconducting states for a generic Gross-Neveu theory with arbitrary spinor components and critical boson modes. These pairing rules should also be useful for numerical investigations of superconductivity near GN criticality. Even if the actual superconducting transition temperature is too low to be accessed in quantum Monte Carlo simulations, one can still analyze the pairing susceptibility in the normal state. This analysis can be carried out for all possible pairing channels, characterized by its spinor structure encoded in Γ^r_J. For those channels that satisfy our pairing rules, we expect the pairing susceptibility to increase much more strongly with decreasing temperature than in all other channels.

Since our theory was formulated for a generic representation of the Dirac matrices, it is instructive to discuss it in the context of a specific realization. To this end we consider

$$\alpha_1 = -\tau_2\sigma_2,\ \alpha_2 = \tau_2\sigma_1,\ \alpha_3 = -\tau_1\sigma_0 \text{ and } \beta = \tau_3\sigma_0, \quad (96)$$

discussed in Refs. [97,98]. Here τ_a stands for two orbitals of opposite parity while σ_b acts in spin space. For this problem it holds that the parity operation is $u_P = \beta$ while time reversal is given as $u_T = i\tau_3\sigma_2$. The pairing states for the four distinct Yukawa couplings, i.e., the interaction terms $\sim g\psi^\dagger\Upsilon_i\psi\phi$ in the action can then easily be analyzed with the help of Table I. The coupling

$$\Upsilon_1 = \gamma^0 = \tau_3\sigma_0, \quad (97)$$

which is even under inversion and time reversal and corresponds to an excitation in the charge channel, describes an orbital fluctuation. For the superconducting gap function induced by this coupling it follows that

$$\Delta(k) = \chi(K)u_T = -i\chi(K)\tau_3\sigma_2, \quad (98)$$

i.e., we obtain a spin-singlet, orbital triplet that is out of phase for the two orbitals. The coupling

$$\Upsilon_2 = i\gamma^0\gamma^3 = -\tau_1\sigma_0, \quad (99)$$

which is odd under parity and TR, and hence corresponds to a toroidal moment. It is trivial in spin space but describes transitions between the orbital states that amount to orbital currents, i.e., some form of loop currents of the two-orbital problem. For the superconducting gap function induced by this coupling follows as

$$\Delta(k) = \chi(K)\gamma^3 u_T = -\chi(K)\tau_1\sigma_2. \quad (100)$$

Hence, we obtain a different spin-singlet / orbital triplet state. The coupling

$$\Upsilon_4 = i\gamma^0\gamma^5 = \tau_2\sigma_2, \quad (101)$$

is also odd under parity and time-reversal and describes spin-orbit entangled toroidal moment. For the superconducting gap function induced by this coupling follows as

$$\Delta(k) = \chi(K)\gamma^5 u_T = i\chi(K)\tau_2\sigma_1. \quad (102)$$

This corresponds to an orbital singlet and spin triplet state. Finally the absence of superconductivity due to

$$\Upsilon_3 = i\gamma^1\gamma^2 = -\tau_0\sigma_3, \quad (103)$$

which is odd under time reversal and even under parity and describes with Eq. (96) spin-ferromagnetic fluctuations, shows that not all Gross-Neveu interactions serve equally efficient as pairing glue. This interaction is most attractive in the channel with the three-component gap function

$$\begin{aligned}\Delta(k) &= \sum_{\mu=0}^{2} \chi^\mu(K)\gamma^\mu u_T, \\ &= -i\chi^0(K)\tau_0\sigma_2 - \chi^1(K)\tau_2\sigma_0 + i\chi^2(K)\tau_2\sigma_3, \end{aligned} \quad (104)$$

which transforms under a three-dimensional irreducible representation. It is a combination of an orbital triplet and spin singlet, with amplitude $\chi^0(K)$ with two orbital singlets / spin triplets, with amplitudes $\chi^{1,2}$. While superconducting fluctuations may be sizable, the pairing interaction does not reach the threshold value in this pairing channel.

The choice of Dirac matrices in Eq. (96) illustrates the rich physics of unconventional pairing states that emerge upon exchanging critical mass-generating bosons in Dirac systems. Our formalism can be readily applied to generic representations of Dirac matrices, allowing one to analyze whether, for a given system, the relevant collective boson can induce pairing and to determine the resulting pairing symmetry. In a subsequent publication [70] the approach will be applied to the case of 8×8 Dirac spinors that describe AB-BA stacked

twisted double-layer WSe_2 at filling $\nu = 2$ [10–14] and to 16×16 Dirac matrices that one encounters in the context of twisted bilayer graphene [35–38,40,41].

Let us also comment on the emergence of superconductivity, induced by TR and parity-odd fluctuations that do not break translation. Recently it was pointed out that such a collective boson is unable to induce superconductivity in the critical regime [98–101]. We emphasize that these restrictions apply only to systems without spin-orbit coupling and therefore do not pertain to our problem.

Finally, we discussed the role of superconducting order-parameter fluctuations beyond the large-N limit, concluding that such fluctuations are likely to reduce the transition temperature but should not destroy the superconducting state identified here. Solving the pairing problem below T_c, addressing the robustness of pairing against disorder and externally applied magnetic fields, and elucidating the connection to topological superconductivity due to charged skyrmions, as discussed in Refs. [42,65–69], are among the important open problems that emerge from our findings.

ACKNOWLEDGMENTS

We are grateful to E. Altman, A. V. Chubukov, L. Classen, I. Esterlis, J. Kim, A. Klein, E. König, G. Palle, N. Parthenios, J. Ruhman, and M. Scheurer for helpful discussions. This work was supported by the German Research Foundation TRR 288-422213477 ELASTO-Q-MAT, B01 (V.C.S. and J.S.) and Grant No. SFI-MPS- NFS-00006741-05 from the Simons Foundation (J.S.). D.E.S. acknowledges support from the National Science Foundation under Grant No. PHY-2208036.

DATA AVAILABILITY

The data that support the findings of this article are openly available [102].

[1] T. O. Wehling, A. M. Black-Schaffer, and A. V. Balatsky, Dirac materials, Adv. Phys. **63**, 1 (2014).

[2] O. Vafek and A. Vishwanath, Dirac fermions in solids: from high-T_c cuprates and graphene to topological insulators and Weyl semimetals, Annu. Rev. Condens. Matter Phys. **5**, 83 (2014).

[3] R. Boyack, H. Yerzhakov, and J. Maciejko, Quantum phase transitions in Dirac fermion systems, Eur. Phys. J. **230**, 979 (2021).

[4] K. S. Novoselov, A. K. Geim, S. V. Morozov, D. Jiang, Y. Zhang, S. V. Dubonos, I. V. Grigorieva, and A. A. Firsov, Electric field effect in atomically thin carbon films, Science **306**, 666 (2004).

[5] A. H. Castro Neto, F. Guinea, N. M. R. Peres, K. S. Novoselov, and A. K. Geim, The electronic properties of graphene, Rev. Mod. Phys. **81**, 109 (2009).

[6] G. Li, A. Luican, J. Lopes dos Santos, A. Castro Neto, A. Reina, J. Kong, and E. Andrei, Observation of Van Hove singularities in twisted graphene layers, Nat. Phys. **6**, 109 (2010).

[7] Y. Cao, V. Fatemi, A. Demir, S. Fang, S. L. Tomarken, J. Y. Luo, J. D. Sanchez-Yamagishi, K. Watanabe, T. Taniguchi, E. Kaxiras, *et al.*, Correlated insulator behaviour at half-filling in magic-angle graphene superlattices, Nature (London) **556**, 80 (2018).

[8] Y. Cao, V. Fatemi, S. Fang, K. Watanabe, T. Taniguchi, E. Kaxiras, and P. Jarillo-Herrero, Unconventional superconductivity in magic-angle graphene superlattices, Nature (London) **556**, 43 (2018).

[9] E. Y. Andrei and A. H. MacDonald, Graphene bilayers with a twist, Nat. Mater. **19**, 1265 (2020).

[10] M. Angeli and A. H. MacDonald, γ valley transition metal dichalcogenide moiré bands, Proc. Natl. Acad. Sci. **118**, e2021826118 (2021).

[11] H. Pan, E.-A. Kim, and C.-M. Jian, Realizing a tunable honeycomb lattice in ABBA-stacked twisted double bilayer WSe_2, Phys. Rev. Res. **5**, 043173 (2023).

[12] B. A. Foutty, J. Yu, T. Devakul, C. R. Kometter, Y. Zhang, K. Watanabe, T. Taniguchi, L. Fu, and B. E. Feldman, Tunable spin and valley excitations of correlated insulators in γ-valley moiré bands, Nat. Mater. **22**, 731 (2023).

[13] L. Ma, R. Chaturvedi, P. X. Nguyen, K. Watanabe, T. Taniguchi, K. F. Mak, and J. Shan, Relativistic Mott transition in twisted WSe_2 tetralayers, Nat. Mater. **24**, 1935 (2025).

[14] M. Tolosa-Simeón, L. Classen, and M. M. Scherer, Relativistic Mott transitions and finite-temperature effects of quantum criticality in Dirac semimetals, Phys. Rev. B **112**, 115133 (2025).

[15] M. Z. Hasan and C. L. Kane, Colloquium: Topological insulators, Rev. Mod. Phys. **82**, 3045 (2010).

[16] X.-L. Qi and S.-C. Zhang, Topological insulators and superconductors, Rev. Mod. Phys. **83**, 1057 (2011).

[17] V. Kozii, Z. Bi, and J. Ruhman, Superconductivity near a ferroelectric quantum critical point in ultralow-density Dirac materials, Phys. Rev. X **9**, 031046 (2019).

[18] V. Kozii, A. Klein, R. M. Fernandes, and J. Ruhman, Synergetic ferroelectricity and superconductivity in zero-density Dirac semimetals near quantum criticality, Phys. Rev. Lett. **129**, 237001 (2022).

[19] G. Montambaux, F. Piéchon, J.-N. Fuchs, and M. O. Goerbig, Merging of Dirac points in a two-dimensional crystal, Phys. Rev. B **80**, 153412 (2009).

[20] H. Isobe, B.-J. Yang, A. Chubukov, J. Schmalian, and N. Nagaosa, Emergent nonFermi-liquid at the quantum critical point of a topological phase transition in two dimensions, Phys. Rev. Lett. **116**, 076803 (2016).

[21] G. Y. Cho and E.-G. Moon, Novel quantum criticality in two dimensional topological phase transitions, Sci. Rep. **6**, 19198 (2016).

[22] J. M. Link, B. N. Narozhny, E. I. Kiselev, and J. Schmalian, Out-of-bounds hydrodynamics in anisotropic Dirac fluids, Phys. Rev. Lett. **120**, 196801 (2018).

[23] D. J. Gross and A. Neveu, Dynamical symmetry breaking in asymptotically free field theories, Phys. Rev. D **10**, 3235 (1974).

[24] J. Zinn-Justin, Four-fermion interaction near four dimensions, Nucl. Phys. B **367**, 105 (1991).

[25] I. F. Herbut, Interactions and phase transitions on graphene's honeycomb lattice, Phys. Rev. Lett. **97**, 146401 (2006).
[26] I. F. Herbut, V. Juričić, and B. Roy, Theory of interacting electrons on the honeycomb lattice, Phys. Rev. B **79**, 085116 (2009).
[27] I. F. Herbut, V. Juričić, and O. Vafek, Relativistic Mott criticality in graphene, Phys. Rev. B **80**, 075432 (2009).
[28] V. Juričić, I. F. Herbut, and G. W. Semenoff, Coulomb interaction at the metal-insulator critical point in graphene, Phys. Rev. B **80**, 081405 (2009).
[29] C. Weeks and M. Franz, Interaction-driven instabilities of a Dirac semimetal, Phys. Rev. B **81**, 085105 (2010).
[30] G. W. Semenoff, Chiral symmetry breaking in graphene, Phys. Scr. **T146**, 014016 (2012).
[31] F. F. Assaad and I. F. Herbut, Pinning the order: the nature of quantum criticality in the Hubbard model on honeycomb lattice, Phys. Rev. X **3**, 031010 (2013).
[32] S. Han and E.-G. Moon, Long-range coulomb interaction effects on the topological phase transitions between semimetals and insulators, Phys. Rev. B **97**, 241101 (2018).
[33] B. Ihrig, L. N. Mihaila, and M. M. Scherer, Critical behavior of Dirac fermions from perturbative renormalization, Phys. Rev. B **98**, 125109 (2018).
[34] T. C. Lang and A. M. Läuchli, Quantum monte carlo simulation of the chiral Heisenberg Gross-Neveu-Yukawa phase transition with a single Dirac cone, Phys. Rev. Lett. **123**, 137602 (2019).
[35] N. Parthenios and L. Classen, Twisted bilayer graphene at charge neutrality: Competing orders of SU(4) Dirac fermions, Phys. Rev. B **108**, 235120 (2023).
[36] J. Biedermann and L. Janssen, Twist-tuned quantum criticality in moiré bilayer graphene, Phys. Rev. B **112**, L041109 (2025).
[37] B. Hawashin, M. M. Scherer, and L. Janssen, Gross-Neveu-XY quantum criticality in moiré Dirac materials, Phys. Rev. B **111**, 205129 (2025).
[38] C. Huang, N. Parthenios, M. Ulybyshev, X. Zhang, F. F. Assaad, L. Classen, and Z. Y. Meng, Angle-tuned Gross-Neveu quantum criticality in twisted bilayer graphene, Nat. Commun. **16**, 7176 (2025).
[39] T. C. Lang and A. M. Läuchli, Chiral Heisenberg Gross-Neveu-Yukawa criticality: Honeycomb vs. SLAC fermions, Phys. Rev. B **112**, 245121 (2025).
[40] N. Bultinck, E. Khalaf, S. Liu, S. Chatterjee, A. Vishwanath, and M. P. Zaletel, Ground state and hidden symmetry of magic-angle graphene at even integer filling, Phys. Rev. X **10**, 031034 (2020).
[41] S. Liu, E. Khalaf, J. Y. Lee, and A. Vishwanath, Nematic topological semimetal and insulator in magic-angle bilayer graphene at charge neutrality, Phys. Rev. Res. **3**, 013033 (2021).
[42] P. J. Ledwith, E. Khalaf, and A. Vishwanath, Strong coupling theory of magic-angle graphene: A pedagogical introduction, Ann. Phys. **435**, 168646 (2021).
[43] K. P. Nuckolls, R. L. Lee, M. Oh, D. Wong, T. Soejima, J. P. Hong, D. Călugăru, J. Herzog-Arbeitman, B. A. Bernevig, K. Watanabe, *et al.*, Quantum textures of the many-body wavefunctions in magic-angle graphene, Nature (London) **620**, 525 (2023).
[44] S. Chandrasekharan and A. Li, Quantum critical behavior in three dimensional lattice Gross-Neveu models, Phys. Rev. D **88**, 021701 (2013).
[45] L. Iliesiu, F. Kos, D. Poland, S. S. Pufu, and D. Simmons-Duffin, Bootstrapping 3D fermions with global symmetries, J. High Energy Phys. 01 (2018) 036.
[46] G. P. Vacca and L. Zambelli, Multimeson Yukawa interactions at criticality, Phys. Rev. D **91**, 125003 (2015).
[47] B. Knorr, Ising and Gross-Neveu model in next-to-leading order, Phys. Rev. B **94**, 245102 (2016).
[48] J. Kim, E. Altman, and X. Cao, Dirac fast scramblers, Phys. Rev. B **103**, L081113 (2021).
[49] S. Sachdev and J. Ye, Gapless spin-fluid ground state in a random quantum Heisenberg magnet, Phys. Rev. Lett. **70**, 3339 (1993).
[50] A. Georges, O. Parcollet, and S. Sachdev, Mean field theory of a quantum Heisenberg spin glass, Phys. Rev. Lett. **85**, 840 (2000).
[51] S. Sachdev, Holographic metals and the fractionalized Fermi liquid, Phys. Rev. Lett. **105**, 151602 (2010).
[52] A. Kitaev, *Talks at KITP, University of California, Santa Barbara, Entanglement in Strongly-Correlated Quantum Matter* (2015).
[53] I. Esterlis and J. Schmalian, Cooper pairing of incoherent electrons: an electron-phonon version of the Sachdev-Ye-Kitaev model, Phys. Rev. B **100**, 115132 (2019).
[54] Y. Wang, Solvable strong-coupling quantum-dot model with a nonFermi-liquid pairing transition, Phys. Rev. Lett. **124**, 017002 (2020).
[55] D. Hauck, M. J. Klug, I. Esterlis, and J. Schmalian, Eliashberg equations for an electron-phonon version of the Sachdev-Ye-Kitaev model: Pair breaking in nonFermi liquid superconductors, Ann. Phys. **417**, 168120 (2020).
[56] I. Esterlis and J. Schmalian, Quantum critical Eliashberg theory, arXiv:2506.11952.
[57] J. Maldacena, S. H. Shenker, and D. Stanford, A bound on chaos, J. High Energy Phys. 08 (2016) 106.
[58] D. Chowdhury, Y. Werman, E. Berg, and T. Senthil, Translationally invariant nonFermi-liquid metals with critical Fermi surfaces: Solvable models, Phys. Rev. X **8**, 031024 (2018).
[59] D. Chowdhury and E. Berg, Intrinsic superconducting instabilities of a solvable model for an incoherent metal, Phys. Rev. Res. **2**, 013301 (2020).
[60] I. Esterlis, H. Guo, A. A. Patel, and S. Sachdev, Large-N theory of critical Fermi surfaces, Phys. Rev. B **103**, 235129 (2021).
[61] A. A. Patel, H. Guo, I. Esterlis, and S. Sachdev, Universal theory of strange metals from spatially random interactions, Science **381**, 790 (2023).
[62] C. Li, D. Valentinis, A. A. Patel, H. Guo, J. Schmalian, S. Sachdev, and I. Esterlis, Strange metal and superconductor in the two-dimensional Yukawa-Sachdev-Ye-Kitaev model, Phys. Rev. Lett. **133**, 186502 (2024).
[63] N. B. Kopnin and E. B. Sonin, BCS superconductivity of Dirac electrons in graphene layers, Phys. Rev. Lett. **100**, 246808 (2008).
[64] O. Abah and M. N. Kiselev, Thermodynamic properties of the superconductivity in quasi-two-dimensional Dirac electronic systems, Eur. Phys. J. B **82**, 47 (2011).

[65] P. B. Wiegmann, Topological electronic liquids: Electronic physics of one dimension beyond the one spatial dimension, Phys. Rev. B **59**, 15705 (1999).

[66] A. Abanov and P. B. Wiegmann, Theta-terms in nonlinear sigma-models, Nucl. Phys. B **570**, 685 (2000).

[67] T. Grover and T. Senthil, Topological spin Hall states, charged skyrmions, and superconductivity in two dimensions, Phys. Rev. Lett. **100**, 156804 (2008).

[68] M. Christos, S. Sachdev, and M. S. Scheurer, Superconductivity, correlated insulators, and Wess-Zumino-Witten terms in twisted bilayer graphene, Proc. Natl. Acad. Sci. **117**, 29543 (2020).

[69] E. Khalaf, S. Chatterjee, N. Bultinck, M. P. Zaletel, and A. Vishwanath, Charged skyrmions and topological origin of superconductivity in magic-angle graphene, Sci. Adv. **7**, eabf5299 (2021).

[70] V. C. Stangier, M. S. Scheurer, D. E. Sheehy, and J. Schmalian, Superconductivity near the relativistic Mott transition in twisted Dirac materials, arXiv:2510.06313.

[71] B. Thaller, *The Dirac Equation* (Springer Science & Business Media, New York, 2013).

[72] J. F. Nieves and P. B. Pal, Generalized Fierz identities, Am. J. Phys. **72**, 1100 (2004).

[73] M. Sigrist and K. Ueda, Phenomenological theory of unconventional superconductivity, Rev. Mod. Phys. **63**, 239 (1991).

[74] A. Abanov, A. V. Chubukov, and A. M. Finkel'stein, Coherent vs. incoherent pairing in 2D systems near magnetic instability, Europhys. Lett. **54**, 488 (2001).

[75] A. Abanov, A. V. Chubukov, and J. Schmalian, Quantum-critical superconductivity in underdoped cuprates, Europhys. Lett. **55**, 369 (2001).

[76] A. V. Chubukov and J. Schmalian, Superconductivity due to massless boson exchange in the strong-coupling limit, Phys. Rev. B **72**, 174520 (2005).

[77] A. Abanov and A. V. Chubukov, Interplay between superconductivity and nonFermi liquid at a quantum critical point in a metal. I. the γ model and its phase diagram at $t = 0$: The case $0 < \gamma < 1$, Phys. Rev. B **102**, 024524 (2020).

[78] Y.-M. Wu, A. Abanov, Y. Wang, and A. V. Chubukov, Interplay between superconductivity and nonFermi liquid at a quantum critical point in a metal. II. the γ model at a finite t for $0 < \gamma < 1$, Phys. Rev. B **102**, 024525 (2020).

[79] Y.-M. Wu, A. Abanov, and A. V. Chubukov, Interplay between superconductivity and nonFermi liquid behavior at a quantum critical point in a metal. III. the γ model and its phase diagram across $\gamma = 1$, Phys. Rev. B **102**, 094516 (2020).

[80] Y.-M. Wu, S.-S. Zhang, A. Abanov, and A. V. Chubukov, Interplay between superconductivity and nonFermi liquid at a quantum critical point in a metal. IV. the γ model and its phase diagram at $1 < \gamma < 2$, Phys. Rev. B **103**, 024522 (2021).

[81] Y.-M. Wu, S.-S. Zhang, A. Abanov, and A. V. Chubukov, Interplay between superconductivity and nonFermi liquid behavior at a quantum-critical point in a metal. V. the γ model and its phase diagram: The case $\gamma = 2$, Phys. Rev. B **103**, 184508 (2021).

[82] R. Ojajärvi, A. V. Chubukov, Y.-C. Lee, M. Garst, and J. Schmalian, Pairing at a single Van Hove point, npj Quantum Mater. **9**, 105 (2024).

[83] Y. Wang and A. V. Chubukov, BCS-like T_c does not necessarily imply BCS pairing mechanism: The case of magnetically mediated quantum critical pairing, Phys. Rev. B **111**, 214514 (2025).

[84] D. B. Kaplan, J.-W. Lee, D. T. Son, and M. A. Stephanov, Conformality lost, Phys. Rev. D **80**, 125005 (2009).

[85] M. Christos, S. Sachdev, and M. S. Scheurer, Nodal band-off-diagonal superconductivity in twisted graphene superlattices, Nat. Commun. **14**, 7134 (2023).

[86] B. Roy and V. Juričić, Unconventional superconductivity in nearly flat bands in twisted bilayer graphene, Phys. Rev. B **99**, 121407 (2019).

[87] A. L. Szabó and B. Roy, Extended hubbard model in undoped and doped monolayer and bilayer graphene: Selection rules and organizing principle among competing orders, Phys. Rev. B **103**, 205135 (2021).

[88] V. L. Berezinskii, Destruction of long-range order in one-dimensional and two-dimensional systems having a continuous symmetry group I. classical systems, Sov. Phys. JETP **32**, 493 (1971).

[89] J. M. Kosterlitz and D. J. Thouless, Ordering, metastability and phase transitions in two-dimensional systems, J. Phys. C: Solid State Phys. **6**, 1181 (1973).

[90] B. Halperin and D. R. Nelson, Resistive transition in superconducting films, J. Low Temp. Phys. **36**, 599 (1979).

[91] Z. M. Raines, S.-S. Zhang, and A. V. Chubukov, Superfluid stiffness within Eliashberg theory: the role of vertex corrections, Phys. Rev. B **109**, 144505 (2024).

[92] R. A. Ferrell and R. E. Glover, Conductivity of superconducting films: A sum rule, Phys. Rev. **109**, 1398 (1958).

[93] M. Tinkham and R. A. Ferrell, Determination of the superconducting skin depth from the energy gap and sum rule, Phys. Rev. Lett. **2**, 331 (1959).

[94] J. Sabio, J. Nilsson, and A. H. Castro Neto, f-sum rule and unconventional spectral weight transfer in graphene, Phys. Rev. B **78**, 075410 (2008).

[95] L. Fritz, J. Schmalian, M. Müller, and S. Sachdev, Quantum critical transport in clean graphene, Phys. Rev. B **78**, 085416 (2008).

[96] G. A. Inkof, J. Küppers, J. M. Link, B. Goutéraux, and J. Schmalian, Quantum critical scaling and holographic bound for transport coefficients near Lifshitz points, J. High Energy Phys. 11 (2020) 088.

[97] C.-X. Liu, X.-L. Qi, H. Zhang, X. Dai, Z. Fang, and S.-C. Zhang, Model Hamiltonian for topological insulators, Phys. Rev. B **82**, 045122 (2010).

[98] G. Palle and J. Schmalian, Unconventional superconductivity from electronic dipole fluctuations, Phys. Rev. B **110**, 104516 (2024).

[99] Z. D. Shi, D. V. Else, H. Goldman, and T. Senthil, Loop current fluctuations and quantum critical transport, SciPost Phys. **14**, 113 (2023).

[100] G. Palle, R. Ojajärvi, R. M. Fernandes, and J. Schmalian, Superconductivity due to fluctuating loop currents, Sci. Adv. **10**, eadn3662 (2024).

[101] D. J. Schultz, G. Palle, Y. B. Kim, R. M. Fernandes, and J. Schmalian, Superconductivity in Kagome metals due to soft loop-current fluctuations, arXiv:2507.16892.

[102] V. C. Stangier, D. E. Sheehy, and J. Schmalian, Data: Strong-coupling superconductivity near Gross-Neveu quantum criticality in Dirac systems, RADAR4KIT (2026).